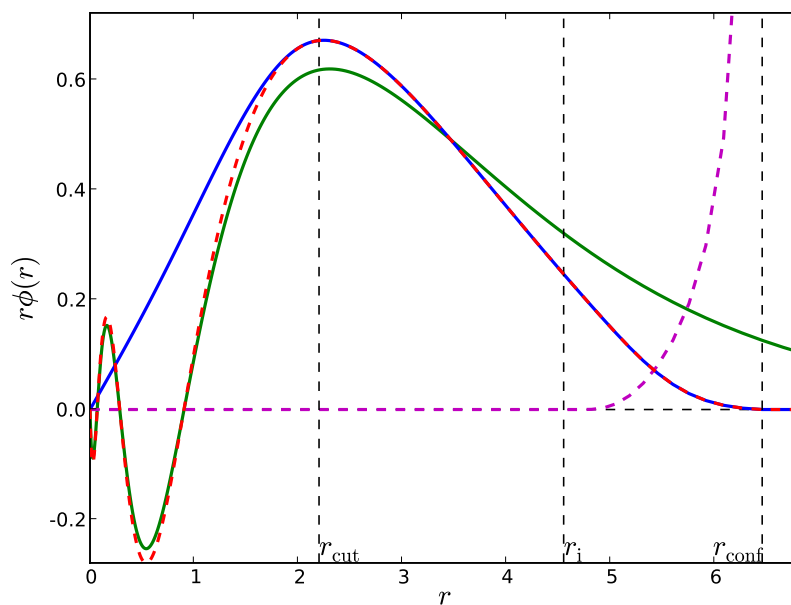


# Localized Atomic Orbital Basis Sets in the Projector Augmented Wave Method



---

Ask Hjorth Larsen, s021864  
Version 1.1. June 24, 2008

Supervisors:  
**Kristian Sommer Thygesen**  
**Jens Jørgen Mortensen**

Center for Atomic-scale Materials Design  
Department of Physics  
Technical University of Denmark

Front cover: Basis function generation for the isolated copper atom (see Chapter 5). The 4s orbital of the free atom (green), the corresponding localized orbital (red, dashed) in the presence of a spherical potential (purple, dashed), and finally the pseudo wave function (blue), which can be used as a basis function.

# Abstract

This thesis concerns the application of localized atom-centered basis functions in the projector augmented wave method. Localized basis sets allow calculations to be performed on considerably larger systems compared to the usual grid or plane-wave methods. We describe the transition from the generic PAW formalism to basis set calculations, resulting in modifications to the Kohn-Sham eigenvalue problem.

Basis functions are implemented as numerical pseudo-atomic orbitals, and methods are described for expanding the basis set with multiple-zeta and polarization functions to improve basis set flexibility. Generated basis sets are tested by comparison of atomization and adsorption energies to accurate grid-based calculations.

Finally an expression for the force affecting an atom is derived and implemented, thus allowing structure relaxations and molecular dynamics simulations.



# Preface

This master thesis was written between September 2007 and June 2008 at the Center for Atomic-scale Materials Design, DTU, Lyngby. Most of the work herein has been performed in close collaboration with Marco Vanin, whom I would like to thank sincerely for the numerous long and helpful discussions along the way.

I am very grateful to my supervisors Kristian Sommer Thygesen and Jens Jørgen Mortensen for all the both physics-related and technical assistance so readily provided throughout the year. Thanks also to Karsten Wedel Jacobsen for advice and active participation in the “basis set meetings”, to Vivien Petzold for supplying the geometries for the adsorption energy calculations, and to my office mates Jens Hummelshøj, Isabela Man, Ture Munter and Poul Georg Moses who have been providing such a pleasant working environment. Poul Georg has also helped proofread the report. Finally, thanks to my parents Ole and Ulla who have been so very helpful, particularly in the final chaotic weeks before finishing the project.



# Contents

<b>Abstract</b>	<b>iii</b>
<b>Preface</b>	<b>v</b>
<b>1 Introduction</b>	<b>1</b>
<b>2 Quantum mechanical background</b>	<b>3</b>
2.1 Many-body Schrödinger equation . . . . .	3
2.2 Density functional theory . . . . .	4
2.3 Kohn-Sham ansatz . . . . .	5
2.4 Iterative solution scheme . . . . .	7
2.5 Exchange and correlation . . . . .	7
2.6 From pseudopotentials to the PAW method . . . . .	8
2.7 Conclusion . . . . .	9
<b>3 The projector augmented wave method</b>	<b>11</b>
3.1 Overview . . . . .	11
3.2 The PAW transformation . . . . .	11
3.3 Operators and expectation values . . . . .	13
3.3.1 Electron density . . . . .	15
3.3.2 Coulomb interaction . . . . .	16
3.3.3 Exchange-correlation functional . . . . .	18
3.3.4 The zero potential . . . . .	18
3.3.5 Total energy . . . . .	18
3.4 The PAW Hamiltonian . . . . .	19
3.5 Modified variational problem . . . . .	20
<b>4 Atomic basis sets</b>	<b>23</b>
4.1 Background . . . . .	23
4.2 Localized functions . . . . .	24
4.3 Two-center integrals . . . . .	24
4.4 Matrix formulation . . . . .	26
4.5 Variational problem . . . . .	28
<b>5 Basis set generation</b>	<b>29</b>
5.1 Overview of atomic basis sets . . . . .	29
5.2 Atomic orbital calculation . . . . .	30
5.2.1 Confinement scheme . . . . .	31
5.2.2 Pseudo orbital calculation . . . . .	32

5.2.3	Confinement radius selection by energy shift . . . . .	36
5.3	Multiple-zeta basis sets . . . . .	37
5.3.1	Energy derivative approach . . . . .	38
5.4	Polarization functions . . . . .	39
5.4.1	Methods for selecting polarization functions . . . . .	40
5.4.2	Wave function interpolation using Gaussians . . . . .	40
5.4.3	Generated functions . . . . .	42
5.4.4	Single-Gaussian polarization functions . . . . .	43
5.5	Basis set parameters in practice . . . . .	44
5.5.1	Notes on state selection . . . . .	46
<b>6</b>	<b>Basis set test results</b>	<b>47</b>
6.1	Molecule tests . . . . .	47
6.2	Adsorption energies . . . . .	48
6.3	Conclusion . . . . .	50
<b>7</b>	<b>Force calculations in LCAO</b>	<b>53</b>
7.1	Strategic considerations . . . . .	53
7.2	Evaluation of force contributions . . . . .	55
7.2.1	State operator contribution . . . . .	55
7.2.2	Kinetic energy contribution . . . . .	56
7.2.3	Compensation charge contribution . . . . .	56
7.2.4	Pseudo density contribution . . . . .	56
7.2.5	Zero potential contribution . . . . .	57
7.2.6	Atomic density contribution . . . . .	57
7.3	General force expression . . . . .	58
7.4	Derivatives of two-center integrals . . . . .	58
7.5	Force test calculations . . . . .	60
7.5.1	Finite-difference checks . . . . .	60
7.5.2	Egg-box forces . . . . .	62
7.6	Summary . . . . .	62
<b>8</b>	<b>Conclusion</b>	<b>65</b>
	<b>Bibliography</b>	<b>67</b>



# List of Figures

5.1	The all-electron Kohn-Sham wave functions for copper. . . . .	32
5.2	The atomic orbital confinement scheme. The red curve corresponds to the unbounded wave function, while the green curve shows the wave function confined in a discontinuous infinite potential well. The blue curve is the smoothly confined wave function obtained by using the dashed potential. . . . .	33
5.3	Pseudo basis function for the sodium 3s orbital calculated using the full expansion expression (5.10), the pseudo-partial wave expansion (5.11) and the weighted expansion (5.12), the latter being well-behaved both near and far from the atom. Note that the wave functions are <i>not</i> premultiplied by $r$ . . . . .	35
5.4	Summary of first-zeta basis function generation. The all-electron solution is localized using a confining potential, then transformed to a pseudo wave function. . . . .	35
5.5	Miscellaneous PAOs for the fixed energy shift 0.3 eV. Lines are coloured by atomic species and styled depending on angular momentum. . . . .	36
5.6	Generation of extra radial functions. The split radius is most practically determined by specifying the norm of the single-zeta tail beyond it. . . . .	38
5.7	The energy derivative approach. Shows a first-zeta orbital and second-zeta orbitals corresponding to the infinite hard-wall potential method, a smooth confinement potential and finally an approach where the derivative is taken with respect to the inner cutoff parameter $r_i$ of the potential. . . . .	39
5.8	Polarization functions for oxygen in H <sub>2</sub> O with varying numbers of primitive functions with evenly distributed characteristic radii. . . . .	43
5.9	Miscellaneous polarization functions, some of which are “hunch-backed”. Calculated using reference molecules CH <sub>4</sub> , NH <sub>3</sub> , H <sub>2</sub> O, HF, AlCl <sub>3</sub> and SiO. Each function is composed of four primitive Gaussian-like orbitals. . . . .	44
5.10	Contracted and normalized d-type 4-Gaussian polarization functions for various elements. The overall shape appears to be universal for small $r$ . The dashed line is a hand-fitted quasi-Gaussian. . . . .	45
5.11	Double-zeta polarized basis set for oxygen. This is the canonical type of basis set presently used for serious calculations, generated with default parameters. . . . .	46

- 6.2 CO adsorbed on a bridge site of a Pd (100) surface. This figure shows the basic cell repeated  $3 \times 3$  times. . . . . 50
- 7.1 Egg-box force test for hydrogen with different grid spacings  $h$ . The dots are calculated energies as a function of the sub-resolution displacement  $x$ . The line segments are given by  $E(x) - F(x) dx$  extrapolated around each point. The red/black curves represent grid-based calculations while the blue/green ones use localized basis functions. The energy zero is arbitrary. . . . . 63

# Chapter 1

## Introduction

Many properties of matter, both physical and chemical, are determined by the interactions of electrons. Quantum mechanics can be used to infer any quantity relating to the electronic structure of materials, although only trivial systems can be treated analytically. The advances in computer technology brought about in the recent decades have enabled high-quality numerical *ab-initio*, or first-principles, calculations on systems involving hundreds or thousands of atoms depending on the methods and approximations. Our primary subject will be density functional theory (DFT) calculations, one of the predominant methods in computational quantum mechanics.

A central challenge to numerical calculations is that the oscillatory behaviour of electronic wave functions near nuclei is difficult to represent efficiently. This problem can be dealt with by considering only electronic valence states, representing the screened nuclei by *pseudopotentials*. *Augmented plane-wave* methods are other ways of taking care of the problem, using different methods to represent wave functions in the regions near and far from the nuclei. The *projector augmented wave method* is a generalization of the pseudopotential methods and augmented-wave methods due to P. Blöchl [8]. So far this method has been combined mostly with the use of plane-wave basis sets or real-space grids to represent wave functions [9, 10].

This thesis concerns the implementation of localized basis sets in the projector augmented wave method, specifically in the GPAW code. GPAW is an implementation of the projector augmented wave method based on real-space grids. It is written in the Python and C programming languages and released as part of the CAMP Open Software project [10, 24, 26].

The use of localized basis sets is a trade-off between numerical accuracy and performance. Plane-wave and grid-based methods can represent wave functions with arbitrary precision using sufficiently fine grids, whereas localized basis set methods focus on a few, carefully selected basis functions to improve performance, allowing calculations on much larger systems.

The basis functions are numerical pseudo-atomic orbitals, each consisting of a radial part and a spherical harmonic angular part. In the transition from real-space grid-based calculations to localized basis sets, operators are represented in terms of matrix elements with basis functions. This involves two-center integrals between pairs of basis functions or the corresponding Bloch states [22, p. 309-312].

Basis functions are generated by solving the radially symmetric Schrödinger equation for the isolated atom, then transforming the resulting valence atomic orbitals to get smooth pseudo wave functions as prescribed by the PAW formalism. To improve the basis set, extra radial functions are added for each valence state. Finally, *polarization functions* are added to improve the angular flexibility of the basis set, having symmetries not present among the valence states. We have implemented a method whereby the polarization functions are generated by interpolating the pseudo wave function of a reference molecule or crystal. The reference is calculated using the real-space grid. Observing that the generated wave functions have a similar, almost universal shape, we conclude that they can be reasonably represented by a properly chosen Gaussian-like function.

The basis sets have been tested on a range of systems and compared to the results using the grid basis.<sup>1</sup> Most tests use simple molecules or crystals. We have also performed a more realistic test by calculating adsorption energies for more complicated systems. These calculations are done without correction for basis set superposition errors, which appear to impact the results significantly. Results are likely to improve correspondingly once such a correction has been implemented.

Finally we have derived and implemented an atomic force expression for use with the basis sets. The force expression differs from the real-space grid case because the basis functions are fixed to the atoms. Moving the atoms therefore alters the basis. The atomic force implementation is tested using finite-difference as well as a more advanced *egg-box* force test.

The content of this thesis is organized as follows.

- Chapter 2 presents briefly the prerequisite quantum mechanical theory including density functional theory, focusing on the Kohn-Sham ansatz which is the foundation of the succeeding chapters.
- Chapter 3 describes the projector augmented wave method. This involves the evaluation of pertinent observables and modifications to the Hamiltonian and Kohn-Sham variational problem.
- Chapter 4 introduces localized basis sets and formulates the ensuing changes to the PAW formalism, once again changing the Kohn-Sham problem.
- Chapter 5 describes the methods by which basis sets are generated. This involves the calculation of pseudo-atomic orbitals and the selection of suitable auxiliary basis functions.
- Chapter 6 presents concisely some notable test results from calculations using localized basis sets.
- Chapter 7 concerns the calculation of atomic forces in the PAW method using atom-centered basis functions. Also includes subsequent testing.

---

<sup>1</sup>Further test results are available in the thesis by Marco Vanin[17].

## Chapter 2

# Quantum mechanical background

This chapter will describe the basic prerequisite theory of density functional theory and the Kohn-Sham equations, starting with the transition from many-body systems to the widely applied independent-particle methods.

### 2.1 Many-body Schrödinger equation

Consider the time-independent Schrödinger equation<sup>1</sup> for a system containing a number of atoms and  $N$  electrons,

$$\hat{H}|\Psi\rangle = E|\Psi\rangle, \quad (2.1)$$

where  $\Psi(\mathbf{r}_1, \dots, \mathbf{r}_N) = \Psi(\{\mathbf{r}_n\})$  is the antisymmetric many-body electronic wave function[20, p. 474] for the  $N$  electrons present in the system. Ignoring nuclear kinetic energies<sup>2</sup>, the Hamiltonian for this system is given by the electronic kinetic energy operator plus the Coulomb interaction potentials between all distinct electrons and nuclei, and therefore has the form [19, pp. 52-53]

$$\hat{H} = -\frac{1}{2} \sum_n \nabla_n^2 + v, \quad (2.2)$$

$$v = \frac{1}{2} \sum_{m \neq n} \frac{1}{\|\mathbf{r}_n - \mathbf{r}_m\|} - \sum_{na} \frac{Z^a}{\|\mathbf{R}^a - \mathbf{r}_n\|} + \frac{1}{2} \sum_{a \neq b} \frac{Z^a Z^b}{\|\mathbf{R}^b - \mathbf{R}^a\|}, \quad (2.3)$$

with  $Z^a$  and  $\mathbf{R}^a$  denoting nuclear charges and positions. The full energy (of a pure state, for simplicity)  $E$  is then given by

$$\langle \Psi | \hat{H} | \Psi \rangle = T + E_{\text{int}} + E_{\text{ext}} + E_{\text{nuc}} = E, \quad (2.4)$$

---

<sup>1</sup>From this point on we shall use *Hartree units*, i.e. we define the reduced Planck's constant  $\hbar$ , the elementary charge  $e$ , the electron mass  $m_e$  and the electrostatic constant  $\frac{1}{4\pi\epsilon_0}$  to be 1. This implies that the Bohr radius  $a_0$  and the Hartree energy  $\text{Ha}$  are also 1.

<sup>2</sup>The nuclear kinetic energies, nuclei being overwhelmingly heavier than electrons, can usually be neglected when describing purely electronic behaviour due to the dependence on inverse mass of the kinetic energy operator  $-\frac{1}{2M}\hbar^2\nabla^2$ . This more formally corresponds to working in the limit  $M \rightarrow \infty$ , which is called the *Born-Oppenheimer approximation*. [19, pp. 482-484]

where we introduce the symbols for the expectation values of each term in the Hamiltonian:  $T$  for the kinetic energy,  $E_{\text{int}}$  for the energy of the interacting electrons,  $E_{\text{ext}}$  for the external electronic-nuclear energy and  $E_{\text{nuc}}$  for the (constant for our purposes) nuclear electrostatic energy.

The primary computational obstacle with the many-body wave function is that it requires three coordinates for each electron. If we were to represent it on a grid, memory requirements would be  $\mathcal{O}(\exp N)$ , for which reason this problem has been termed *the exponential wall* [2]. Much work has been invested in developing more computationally feasible *independent-electron* methods, where each electron is assigned a *single-particle* wave function  $\psi_n(\mathbf{r})$ . Generally this involves defining an *effective Hamiltonian*, defining a modified Schrödinger equation from which the wave functions are obtained as the (orthogonal) solutions:

$$\hat{H}_{\text{eff}}\psi_n(\mathbf{r}) = \epsilon_n\psi_n(\mathbf{r}), \quad (2.5)$$

where  $f_n$  are the occupation numbers. The effective Hamiltonian is generally defined by replacing the potential  $v$  by an *effective* potential  $v_{\text{eff}}^\sigma(\mathbf{r})$  which is different for particles with different spins<sup>3</sup>  $\sigma$ , such that the effective Hamiltonian itself becomes spin-dependent:

$$\hat{H}_{\text{eff}}^\sigma = -\frac{1}{2}\nabla^2 + v_{\text{eff}}^\sigma. \quad (2.6)$$

The effective potential takes different forms depending on the methods used. For future convenience, note that for any system of this kind, the state operator is given by [19, p. 62]

$$\hat{\rho} = \sum_n f_n |\psi_n\rangle\langle\psi_n|, \quad (2.7)$$

and the electronic density is

$$n(\mathbf{r}) = \sum_n f_n \psi_n^*(\mathbf{r})\psi_n(\mathbf{r}) = \sum_n f_n \langle\psi_n|\mathbf{r}\rangle\langle\mathbf{r}|\psi_n\rangle. \quad (2.8)$$

These independent-particle expressions are fundamental for many modern electronic structure methods including the PAW method which we will consider later. First, however, we will turn to a different underlying piece of theory, namely *density functional theory*.

## 2.2 Density functional theory

It has been shown by P. Hohenberg and W. Kohn that the electronic density can be regarded as a fundamental, basic variable in place of the wave functions [1]. This has led to the entire field of *density functional theory*. Density functional theory rests on the two *Hohenberg-Kohn theorems* which will be detailed below.

We consider again the many-body Hamiltonian (2.2) with the potential

$$v = v_{\text{ext}} + \sum_{m \neq n} \frac{1}{|\mathbf{r}_n - \mathbf{r}_m|}, \quad (2.9)$$

---

<sup>3</sup>The spin-dependence is necessary to take the Pauli exclusion principle properly into account. If the system under consideration is not spin-polarized, however, this can be ignored except each state will be spin-degenerate and thus doubly occupied.

where  $v_{\text{ext}}$  is the potential due to the nuclei (but can in general include other effects as well). Then the Hohenberg-Kohn theorems state:

- Given the ground state electron density  $n_0$ , the external potential  $v_{\text{ext}}$  is determined uniquely down to a constant.
- There exists a functional  $E_{\text{HK}}[n]$  of the density which is, given  $v_{\text{ext}}$ , globally minimized by the ground state density. The global minimum  $E_0 = E_{\text{HK}}[n_0]$  is equal to the ground state energy.

Since knowing the effective potential determines the entire Hamiltonian and by extension any physical property pertaining to the system, the ground state electron density is, by the first theorem, also sufficient to determine any physical property. The second theorem guarantees that the ground state density can be found by variationally through the ground state density.<sup>4</sup>

Thus, the energy is a functional of the electron density

$$E_{\text{HK}}[n] = T[n] + E_{\text{int}}[n] + E_{\text{ext}}[n] + E_{\text{nuc}}. \quad (2.10)$$

While the Hohenberg-Kohn theorems guarantee that physical properties are determined by the electron density alone, thereby not needing any explicit representation of many- or single-body wave functions, the Hohenberg-Kohn theorems do not provide any explicit way to obtain quantities [19, pp. 131-132]. The *Kohn-Sham ansatz*[3] is a practical approach which considers again an independent-particle system rather than the many-body problem.

## 2.3 Kohn-Sham ansatz

The fundamental assumption of this approach is that there exists an independent-particle system which reproduces the ground state density. Any formulation which is capable of reproducing the exact ground state density is in principle exact by the first Hohenberg-Kohn theorem.

First of all, the interacting-electron functionals  $T[n]$  and  $E_{\text{int}}[n]$  are replaced by the non-interacting kinetic energy  $T_s[n]$  and the energy  $E_{\text{Ha}}[n]$  of the total electron density, called the *Hartree energy*. We further introduce a correction  $E_{\text{xc}}[n]$ , called the *exchange-correlation energy*, which accounts for the interaction effects. This correction is generally chosen as a particular approximation, indeed the *only* inherent approximation, and shall be discussed later. The Hartree energy is given by

$$E_{\text{Ha}}[n] = \frac{1}{2} \int \frac{n(\mathbf{r})n(\mathbf{r}')}{|\mathbf{r} - \mathbf{r}'|} d^3\mathbf{r} d^3\mathbf{r}' = \frac{1}{2} \int n(\mathbf{r})v_{\text{Ha}}(\mathbf{r}) d^3\mathbf{r}, \quad (2.11)$$

with the Hartree potential

$$v_{\text{Ha}}(\mathbf{r}) = \int \frac{n(\mathbf{r}')}{|\mathbf{r} - \mathbf{r}'|} d^3\mathbf{r}'. \quad (2.12)$$

---

<sup>4</sup>Proofs of the Hohenberg-Kohn theorems can be found in [19, pp. 123-125]

By now we can write the total energy as

$$\begin{aligned}
E_0 &= T_s[\{\psi_n\}] + E_{\text{Ha}}[n] + E_{\text{ext}}[n] + E_{\text{xc}}[n] \\
&= \sum_n f_n \langle \psi_n | -\frac{1}{2} \nabla^2 | \psi_n \rangle + \frac{1}{2} \int v_{\text{Ha}}(\mathbf{r}) n(\mathbf{r}) d^3\mathbf{r} \\
&\quad + \int v_{\text{ext}}(\mathbf{r}) n(\mathbf{r}) d^3\mathbf{r} + E_{\text{xc}}[n].
\end{aligned} \tag{2.13}$$

We define the Kohn-Sham Hamiltonian as the functional derivative[20, pp. 290-291] of the Kohn-Sham energy with respect to the conjugate wave function  $\psi_n^*(\mathbf{r})$ . Using that  $\frac{\partial n(\mathbf{r})}{\partial \psi_n^*(\mathbf{r})} = f_n \psi_n(\mathbf{r})$  from Equation (2.8),

$$\begin{aligned}
\frac{\delta E_0}{\delta \psi_n^*(\mathbf{r})} &= -\frac{1}{2} f_n \nabla^2 \psi_n(\mathbf{r}) + \left\{ \frac{\delta E_{\text{Ha}}}{\delta n(\mathbf{r})} + \frac{\delta E_{\text{ext}}}{\delta n(\mathbf{r})} + \frac{\delta E_{\text{xc}}}{\delta n(\mathbf{r})} \right\} \frac{\delta n(\mathbf{r})}{\delta \psi_n^*(\mathbf{r})} \\
&= f_n \left[ -\frac{1}{2} \nabla^2 + v_{\text{Ha}}(\mathbf{r}) + v_{\text{ext}}(\mathbf{r}) + v_{\text{xc}}(\mathbf{r}) \right] \psi_n(\mathbf{r}) \\
&= f_n \hat{H}_{\text{KS}} \psi_n(\mathbf{r}),
\end{aligned} \tag{2.14}$$

where we have defined  $v_{\text{xc}}(\mathbf{r}) = \frac{\delta E_{\text{xc}}[n]}{\delta n(\mathbf{r})}$ . Note that the factor 1/2 in the Hartree term has disappeared due to the implicit quadratic dependence on density. The Hamiltonian thus has the form of a Laplacian plus an effective potential, like (2.6).

To solve this, we formulate a variational problem in  $\psi_n$ , using Lagrange multipliers  $\lambda_{nm}$  to enforce the constraint that the wave functions must be mutually orthogonal:

$$\Omega(\{\psi_n\}, \{\lambda_{nm}\}) = E_0[\{\psi_n\}] - \sum_{mn} \lambda_{mn} (\langle \psi_n | \psi_m \rangle - \delta_{nm}). \tag{2.15}$$

This expression is minimal for the set of orthogonal wave functions that constitutes the ground state. Since the energy functional has to be stationary with respect to the wave functions (and thus the conjugate wave functions) at a minimum, we can set the derivative of  $\Omega$  to zero, obtaining

$$0 = \frac{\delta \Omega}{\delta \psi_n^*(\mathbf{r})} = \frac{\delta E_0}{\delta \psi_n^*(\mathbf{r})} - \sum_{mn} \lambda_{mn} \psi_m(\mathbf{r}), \tag{2.16}$$

or

$$f_n \hat{H}_{\text{KS}} |\psi_n\rangle = \sum_m \lambda_{mn} |\psi_m\rangle. \tag{2.17}$$

Evidently the wave functions  $|\psi_n\rangle$  are not eigenstates of the Hamiltonian until we diagonalize the matrix of Lagrange multipliers, resulting in a set of modified states such that

$$\hat{H}_{\text{KS}} |\psi_n\rangle = \epsilon_n |\psi_n\rangle, \tag{2.18}$$

where we have collapsed the Lagrange multipliers  $\lambda_{nn}$  and occupation numbers<sup>5</sup>  $f_n$  to  $\epsilon_n$ , the *Kohn-Sham energy eigenvalue*. In order for this to be correct, how-

<sup>5</sup>At first sight the exclusion of the occupation numbers appears ill-defined for unoccupied states. Generally the eigenvalue equation is solved without regard for the occupation numbers, simply yielding orthogonal states with yet arbitrary occupation. Occupation numbers are added afterwards by populating the lowest-energy states or generally by means of a Fermi-Dirac distribution to get densities, potentials etc.



ever, we must of course have determined the effective potential which appears in the Hamiltonian, which depends on the still unknown density. All this can be done iteratively, thus arriving at a *self-consistent* state.

## 2.4 Iterative solution scheme

The iterative method used to solve the Kohn-Sham equations will be briefly outlined below. When referring to wave functions, density and effective potential below, those are *provisional estimates* which will converge to *self-consistent* quantities when the algorithm finishes.

Each provisional wave function is initialized using a qualified guess, for example a linear combination of atomic orbitals. The following steps are then repeated until converged:

- The electron density is calculated from the wave functions<sup>6</sup> and occupation numbers (Equation (2.8)).
- The Hartree potential is calculated. This can be done efficiently by solving the Poisson equation<sup>7</sup>  $\nabla^2 v_{\text{Ha}}(\mathbf{r}) = -4\pi n(\mathbf{r})$ , which is more effective than using (2.12) directly.
- The effective potential is calculated by adding the Hartree potential  $v_{\text{Ha}}$ , the external potential  $v_{\text{ext}}$  and the exchange-correlation potential  $v_{\text{xc}}$ .
- The Kohn-Sham equations are solved for the eigenstates cf. (2.18). When using small basis sets, such as localized atomic orbitals, the Hamiltonian can be diagonalized completely. With more parameters, for example when using grid-based wave functions in GPAW, it is more efficient to use an iterative method which runs only partially to completion on each self-consistency iteration.
- The occupation numbers are updated according to the Kohn-Sham energies which are known by (2.18).

This completes the description of the Kohn-Sham ansatz. The only approximation applied is contained within the exchange-correlation functional which we shall discuss next.

## 2.5 Exchange and correlation

The antisymmetry of the electronic many-body wave function leads to a change in physical properties, called the *exchange interaction*, while many-body effects relating to the electronic Coulomb repulsion lead to *correlation*. We shall not describe these interactions thoroughly here. For our purposes it suffices to note that these effects are in general *non-local* and cannot be readily accounted for in independent-particle formulations.

---

<sup>6</sup>In succeeding iterations, it can be necessary to use *density mixing* to improve convergence. Instead of using directly the newly calculated density, this density is set to a normalized, weighted linear combination of the previous densities.

<sup>7</sup>The unusual factor of  $4\pi$  emerges from the vacuum permittivity in Hartree units, the original Poisson equation being  $\nabla^2 v(\mathbf{r}) = -n(\mathbf{r})/\epsilon_0$ .

In the Kohn-Sham scheme, they are grouped together in the *exchange-correlation* functional<sup>8</sup>  $E_{xc}[n]$  written in terms of an exchange-correlation energy density  $\epsilon_{xc}[n](\mathbf{r})$ , such that

$$E_{xc}[n] = \int n(\mathbf{r})\epsilon_{xc}[n](\mathbf{r}) d^3\mathbf{r}. \quad (2.19)$$

The exchange-correlation potential is then defined as

$$v_{xc}(\mathbf{r}) = \frac{\delta E_{xc}[n]}{\delta n(\mathbf{r})} = \epsilon_{xc}[n](\mathbf{r}) + n(\mathbf{r})\frac{\delta\epsilon_{xc}[n]}{\delta n(\mathbf{r})}. \quad (2.20)$$

While  $\epsilon_{xc}[n](\mathbf{r})$  can depend in any way on  $n$ , it is usually assumed to be either fully *local*, meaning that it is characterized purely by the value of the density at  $\mathbf{r}$ , or *semi-local*, meaning that the behaviour of  $n$  in *any* neighbourhood of  $\mathbf{r}$  is sufficient to characterize it.

One of the few cases where exchange and correlation effects can be evaluated exactly is the free electron gas. The *local density approximation*, LDA, approximates the exchange-correlation energy density  $\epsilon_{xc}[n](\mathbf{r})$  in each point with that of a uniform electron gas with the same electron density.

As for semi-local energy functionals, the *generalized gradient approximations*, GGAs, express  $\epsilon_{xc}[n]$  as a function of the value  $n(\mathbf{r})$  and the gradient  $\nabla n(\mathbf{r})$  of the density at  $\mathbf{r}$ . Calculations done in this work generally use either LDA or the PBE functional, a generalized gradient approximation due to Perdew, Burke and Ernzerhof [4].

## 2.6 From pseudopotentials to the PAW method

Owing to the strong attractive potential in the vicinity of a nucleus, electrons will have large kinetic energy densities in this region. This, along with the requirement of wave function orthogonality, causes the electronic wave functions to exhibit swift oscillations near the nucleus. On the contrary, in the interstitial regions between nuclei in a bonding environment, the wave functions are very smooth. This poses a significant problem to computational methods, since the quickly oscillating parts of the wave functions must be represented with very high resolution grids, but this resolution is a waste of memory in the large interstitial regions.

The strongly bound electronic states, being localized close to the nucleus, tend not to contribute appreciably to the bonding properties of elements. Various methods have been formulated which disregard the core electrons, replacing the strong attractive potential of the nucleus with a smooth *pseudopotential* which takes into account the screening effect of the disregarded electronic states. The electronic wave functions calculated using pseudopotentials are generally termed *pseudo wave functions*, and do not exhibit the strong oscillations otherwise found. The original wave functions are then termed *all-electron wave functions*, a nomenclature inherited in the PAW method as well.

Our basis set implementation is very similar to that of the SIESTA code which uses *Kleinman-Bylander* projectors, which are non-local pseudopotentials somewhat reminiscent of the PAW method [11, 6]. An even more advanced method,

<sup>8</sup>In practice this would be the spin-dependent  $E_{xc}[n^\uparrow, n^\downarrow]$ , leading to spin-specific exchange-correlation potentials  $v_{xc}^\uparrow(\mathbf{r})$  and  $v_{xc}^\downarrow(\mathbf{r})$ , though we shall omit these considerations here.

the *ultrasoft* pseudopotentials [5], extending the Kleinman-Bylander potentials, improves the smoothness further by circumventing norm conservation. This is the method used in the Dacapo plane-wave code, developed at CAMD [25]. The *projector augmented wave method* due to Blöchl[8, 9, 7] generalizes the pseudopotential methods, allowing the reconstruction of the all-electron wave functions. This will be the subject of the next chapter.

## 2.7 Conclusion

At this point we have reformulated the troublesome many-body problem into a better-scaling independent-electron formulation which, by the results of density functional theory, is exact down to our approximation of the exchange-correlation functional. We have further outlined a concrete iterative method whereby the Kohn-Sham equations are solved to yield the self-consistent Kohn-Sham wave functions, thus enabling the evaluation of many physical quantities<sup>9</sup>, and provided an overview of existing methods comparable to the PAW method.

---

<sup>9</sup>Since the Kohn-Sham problem is an artificial construct, the resulting wave functions and eigenvalues cannot readily be ascribed a particular physical meaning, and are not guaranteed to predict all physical quantities as can be done with the true wave function.[19, pp. 146-147]



## Chapter 3

# The projector augmented wave method

The *projector augmented wave method*, first proposed by Peter E. Blöchl in 1994[8], is a method for reformulating an ordinary Kohn-Sham problem with numerically inconvenient behaviour into a more computationally digestible form, which involves a different Kohn-Sham problem plus certain corrections. This chapter will describe the PAW method in detail.

### 3.1 Overview

The PAW method proposes to solve the numerical problem of swiftly oscillating wave functions by considering, rather than the all-electron Kohn-Sham problem, a modified problem posed in terms of smooth *pseudo* quantities.

We shall divide the effort to make this method work into three parts. First we must decide on a transformation  $\hat{T}$  between all-electron wave functions  $|\psi_n\rangle$  and pseudo wave functions  $|\tilde{\psi}_n\rangle$ , such that

$$|\psi_n\rangle = \hat{T}|\tilde{\psi}_n\rangle. \quad (3.1)$$

Second, we must obtain a way in which to evaluate the all-electron quantities such as energies and densities from the pseudo quantities.

Third, we must reformulate the variational problem in terms of pseudo wave functions, which will result in a different Hamiltonian and thus different Kohn-Sham equations.

### 3.2 The PAW transformation

Let us consider a transformation which leaves the pseudo wave functions identical to the all-electron ones far from the atoms, while each atom  $a$  imposes a modification described by some operator  $\hat{T}^a$  which is localized to a spherical region, the *augmentation sphere* with *cutoff radius*  $r_c^a$ , around that atom. In the following we require that the augmentation spheres do not overlap. Such an

operator can be written

$$\hat{T} = 1 + \sum_a \hat{T}^a. \quad (3.2)$$

Now, since any operator is completely determined by specifying its action on any basis in definition space in terms of some other basis in image space, we shall choose two basis sets. The natural choice for a basis set for all-electron entities is the set  $\{|\phi_i^a\rangle\}$  of Kohn-Sham atomic orbitals of the isolated atom. For each of these we choose one smooth wave function, obtaining the set  $\{|\tilde{\phi}_i^a\rangle\}$ . Then  $\hat{T}^a$  is completely determined by requiring that each smooth basis function be mapped to one of the all-electron atomic orbitals, such that for all  $i$ ,

$$|\phi_i^a\rangle = (1 + \hat{T}^a)|\tilde{\phi}_i^a\rangle. \quad (3.3)$$

The functions  $|\phi_i^a\rangle$  shall be referred to as *all-electron partial waves* whereas the smooth functions  $|\tilde{\phi}_i^a\rangle$  are termed *pseudo partial waves*. They are chosen such that  $\phi_i^a(\mathbf{r}) = \tilde{\phi}_i^a(\mathbf{r})$  for all  $\mathbf{r}$  outside the local augmentation sphere, which enforces the requirement that the transformation must be unity outside the augmentation sphere.<sup>1</sup> If the pseudo partial waves form a complete set, the pseudo wave function  $\tilde{\psi}_n$  can be expanded as a linear combination of pseudo partial waves. One way to express this is through an arbitrary projection  $\hat{P}$  which has to be the identity operator within the augmentation region. Such a projection operator can be written generally as

$$\hat{P} = \sum_{ij} |\tilde{\phi}_i^a\rangle [O^{-1}]_{ij} \langle f_j^a|, \quad (3.4)$$

where  $\langle f_j^a|$  is a set of functions, as many as there are partial waves, and where  $O_{ji} = \langle f_j^a | \tilde{\phi}_i^a \rangle$  must form a regular matrix. If we define

$$\langle \tilde{p}_i^a | = \sum_j [O^{-1}]_{ij} \langle f_j^a |, \quad (3.5)$$

the partial-wave expansion of the pseudo wave function reads

$$|\tilde{\psi}\rangle = \sum_{ai} |\tilde{\phi}_i^a\rangle \langle \tilde{p}_i^a | \tilde{\psi}\rangle. \quad (3.6)$$

The functions  $|\tilde{p}_i^a\rangle$  are called *projectors*, and each of them is specially associated with a particular pseudo partial wave:

$$\langle \tilde{p}_i^a | \tilde{\phi}_j^a \rangle = \sum_k [O^{-1}]_{ik} \langle f_k^a | \tilde{\phi}_j^a \rangle = [O^{-1}O]_{ij} = \delta_{ij}. \quad (3.7)$$

Thus non-corresponding projectors and the pseudo partial waves are orthogonal. To sum up, *any* choice of linearly independent functions  $|f_i^a\rangle$  thereby corresponds to a set of *projector functions*  $|\tilde{p}_i^a\rangle$  such that the orthogonality condition (3.7) applies.

---

<sup>1</sup>While the formulas presented here presume non-overlapping augmentation regions, modest violations of this requirement will introduce only small errors since the overlapping cross-site quantities are both small near the cutoff.

The relation between all-electron and pseudo wave functions can now be written in terms of  $|\phi_i^a\rangle$ ,  $|\tilde{\phi}_i^a\rangle$  and  $|\tilde{p}_i^a\rangle$ , using (3.2):

$$|\psi\rangle = \hat{T}|\tilde{\psi}\rangle = |\tilde{\psi}\rangle + \sum_a \hat{T}^a|\tilde{\psi}\rangle = |\tilde{\psi}\rangle + \sum_{ai} \hat{T}^a|\tilde{\phi}_i^a\rangle\langle\tilde{p}_i^a|\tilde{\psi}\rangle \quad (3.8)$$

$$= |\tilde{\psi}\rangle + \sum_{ai} \left( |\phi_i^a\rangle - |\tilde{\phi}_i^a\rangle \right) \langle\tilde{p}_i^a|\tilde{\psi}\rangle, \quad (3.9)$$

for which reason the transformation operator has the final form

$$\hat{T} = 1 + \sum_{ai} \left( |\phi_i^a\rangle - |\tilde{\phi}_i^a\rangle \right) \langle\tilde{p}_i^a|. \quad (3.10)$$

We use the *frozen core* approximation, meaning that the core electronic states (generally the largest closed electronic shell) are assumed not to participate in bonding. For this reason, partial waves and projectors are calculated for the valence states, and possibly extra, unoccupied states to improve the partial wave basis.

In conclusion, the computational advantage of using this operator lies in the proposition that one can use a relatively coarse grid in real or reciprocal space to represent the smooth wave function  $|\tilde{\psi}\rangle$ , whereas its interactions with the atoms are separated out as partial wave expansions. The partial waves can then be represented on an atom-centered *radial grid* which does not need to be equidistant. Thus the cumbersome all-electron behaviour can be dealt with by using high radial resolution near the nucleus. Finally the expansion coefficients  $\langle\tilde{p}_i^a|\psi\rangle$ , which constitute the link between the two representations, involve purely smooth functions and are therefore well-behaved too.

### 3.3 Operators and expectation values

Our grand plan is to obtain a Kohn-Sham Hamiltonian which we can use with the iterative scheme from Section 2.4. The Hamiltonian can, like in Section 2.3, be defined through a derivative of the energy expression. Thus we have to derive the energy expression, which requires rewriting several quantities such as electron densities, charge densities and so on in a PAW context. This is the objective of the next sections.

In general, the expectation value of an operator  $\hat{A}$  is

$$\langle\hat{A}\rangle = \sum_n f_n \langle\psi_n|\hat{A}|\psi_n\rangle + \sum_{ac} \langle\phi_c^a|\hat{A}|\phi_c^a\rangle, \quad (3.11)$$

where the subscript  $c$  denotes the frozen core states.<sup>2</sup> The wave functions can be represented in a plane wave basis, on a real-space grid such as in GPAW or as a linear combination of localized functions, though the specifics of the latter case will be dealt with in the next chapter.

We will now rewrite expression for the expectation value in terms of PAW

<sup>2</sup>The spin-degenerate core states are here considered different states altogether, thus avoiding bothersome occupation factors of  $f_c = 2$ .

quantities. Define the one-center wave function contributions

$$|\psi_n^a\rangle = \sum_i |\phi_i^a\rangle \langle \tilde{p}_i^a | \tilde{\psi}_n \rangle, \quad (3.12)$$

$$|\tilde{\psi}_n^a\rangle = \sum_i |\tilde{\phi}_i^a\rangle \langle \tilde{p}_i^a | \tilde{\psi}_n \rangle, \quad (3.13)$$

such that

$$|\psi_n\rangle = |\tilde{\psi}_n\rangle + \sum_a \left( |\psi_n^a\rangle - |\tilde{\psi}_n^a\rangle \right). \quad (3.14)$$

The first bracket in (3.11) is then

$$\begin{aligned} \langle \psi_n | \hat{A} | \psi_n \rangle &= \langle \tilde{\psi}_n | \hat{A} | \tilde{\psi}_n \rangle + \sum_a \left\{ \langle \tilde{\psi}_n | \hat{A} | \psi_n^a - \tilde{\psi}_n^a \rangle + \langle \psi_n^a - \tilde{\psi}_n^a | \hat{A} | \tilde{\psi}_n \rangle \right\} \\ &+ \sum_{ab} \langle \psi_n^a - \tilde{\psi}_n^a | \hat{A} | \psi_n^b - \tilde{\psi}_n^b \rangle. \end{aligned} \quad (3.15)$$

Due to numerical issues, we want to avoid brackets involving both all-electron and pseudo entities. Extracting the diagonal ( $a = b$ ) terms from the last sum and incorporating them into the second and third terms, one eventually obtains

$$\begin{aligned} \langle \psi_n | \hat{A} | \psi_n \rangle &= \langle \tilde{\psi}_n | \hat{A} | \tilde{\psi}_n \rangle + \sum_a \left\{ \langle \psi_n^a | \hat{A} | \psi_n^a \rangle - \langle \tilde{\psi}_n^a | \hat{A} | \tilde{\psi}_n^a \rangle \right\} \\ &+ \sum_a \left\{ \langle \tilde{\psi}_n - \tilde{\psi}_n^a | \hat{A} | \psi_n^a - \tilde{\psi}_n^a \rangle + \langle \psi_n^a - \tilde{\psi}_n^a | \hat{A} | \tilde{\psi}_n - \tilde{\psi}_n^a \rangle \right\} \\ &+ \sum_{a \neq b} \langle \psi_n^a - \tilde{\psi}_n^a | \hat{A} | \psi_n^b - \tilde{\psi}_n^b \rangle. \end{aligned} \quad (3.16)$$

If  $\hat{A}$  is a local operator, the third term is zero, since  $\tilde{\psi}_n(\mathbf{r}) = \sum_a \tilde{\psi}_n^a(\mathbf{r})$  inside the augmentation regions (apart from any side effect of using non-complete pseudo partial waves and projectors), whereas  $\psi_n^a(\mathbf{r}) = \tilde{\psi}_n^a(\mathbf{r})$  outside.

The fourth term, which runs over pairs of distinct atoms, is likewise zero for local operators, since the augmentation regions do not overlap. The one-center matrix elements are equal to

$$\langle \psi_n^a | \hat{A} | \psi_n^a \rangle = \sum_{ij} \langle \tilde{\psi}_n | \tilde{p}_i^a \rangle \langle \phi_i^a | \hat{A} | \phi_j^a \rangle \langle \tilde{p}_j^a | \tilde{\psi}_n \rangle, \quad (3.17)$$

$$\langle \tilde{\psi}_n^a | \hat{A} | \tilde{\psi}_n^a \rangle = \sum_{ij} \langle \tilde{\psi}_n | \tilde{p}_i^a \rangle \langle \tilde{\phi}_i^a | \hat{A} | \tilde{\phi}_j^a \rangle \langle \tilde{p}_j^a | \tilde{\psi}_n \rangle, \quad (3.18)$$

so the full expression for the expectation value is

$$\begin{aligned} \langle \hat{A} \rangle &= \sum_n f_n \langle \tilde{\psi}_n | \hat{A} | \tilde{\psi}_n \rangle + \sum_{n a i j} f_n \langle \tilde{\psi}_n | \tilde{p}_i^a \rangle \langle \phi_i^a | \hat{A} | \phi_j^a \rangle \langle \tilde{p}_j^a | \tilde{\psi}_n \rangle \\ &- \sum_{n a i j} f_n \langle \tilde{\psi}_n | \tilde{p}_i^a \rangle \langle \tilde{\phi}_i^a | \hat{A} | \tilde{\phi}_j^a \rangle \langle \tilde{p}_j^a | \tilde{\psi}_n \rangle + \sum_{ac} \langle \phi_c^a | \hat{A} | \phi_c^a \rangle. \end{aligned} \quad (3.19)$$

The first term involves only the pseudo wave functions on the regular grid, whereas the matrix elements  $\langle \phi_i^a | \hat{A} | \phi_j^a \rangle$  and  $\langle \tilde{\phi}_i^a | \hat{A} | \tilde{\phi}_j^a \rangle$  of the second and the



third terms are evaluated pre-emptively in an atomic context on the radial grid, thus avoiding again any brackets mixing all-electron and pseudo entities. Like in (3.9), the pseudo wave functions interact with the partial wave expansions only through the projections  $\langle \tilde{p}_i^a | \tilde{\psi}_n \rangle$ , which are also numerically convenient.

The link between entities on the regular grid and the radial grid can be expressed in terms of the *atomic density matrices* defined as

$$D_{ij}^a = \sum_n f_n \langle \tilde{p}_i^a | \tilde{\psi}_n \rangle \langle \tilde{\psi}_n | \tilde{p}_j^a \rangle. \quad (3.20)$$

Aside from  $D_{ij}^a$  there are no cross-grid-type integrations. This type of integration is performed by deploying the radial function to the grid, which can be done once and for all at the beginning of a calculation. The expectation value can then be expressed as

$$\begin{aligned} \langle \hat{A} \rangle &= \sum_n f_n \underbrace{\langle \tilde{\psi}_n | \hat{A} | \tilde{\psi}_n \rangle}_{\text{regular grid}} + \sum_{aij} D_{ji}^a \underbrace{\left\{ \langle \phi_i^a | \hat{A} | \phi_j^a \rangle - \langle \tilde{\phi}_i^a | \hat{A} | \tilde{\phi}_j^a \rangle \right\}}_{\text{radial grid}} \\ &+ \sum_{ac} \underbrace{\langle \phi_c^a | \hat{A} | \phi_c^a \rangle}_{\text{radial grid}}. \end{aligned} \quad (3.21)$$

This is straightforward for the kinetic energy, for example, but for other quantities there can be special issues to consider.

### 3.3.1 Electron density

From the electron density (2.8) we separate out the total core state density  $n_c^a(\mathbf{r}) = \sum_c \langle \phi_c^a | \mathbf{r} \rangle \langle \mathbf{r} | \phi_c^a \rangle$  of each atom (this distribution is a radial function of the distance to the atom, but our coordinate system is off-site, so we have to write  $\mathbf{r}$  rather than  $r$ ), so the density including the frozen-core contribution can be written

$$n(\mathbf{r}) = \sum_n f_n \langle \psi_n | \mathbf{r} \rangle \langle \mathbf{r} | \psi_n \rangle + \sum_a n_c^a(\mathbf{r}). \quad (3.22)$$

We cannot expect the core state density to be entirely contained within the augmentation region. Therefore we define a pseudo core state density  $\tilde{n}_c^a(\mathbf{r})$ , which can be any smooth distribution within the augmentation sphere, but must be equal to the all-electron core density outside. Then, since  $|\mathbf{r}\rangle\langle\mathbf{r}|$  is local, we can straightforwardly make use of (3.21) to write the density as

$$n(\mathbf{r}) = \tilde{n}(\mathbf{r}) + \sum_a \{n^a(\mathbf{r}) - \tilde{n}^a(\mathbf{r})\}, \quad (3.23)$$

where

$$\tilde{n}(\mathbf{r}) = \sum_n f_n \langle \tilde{\psi}_n | \mathbf{r} \rangle \langle \mathbf{r} | \tilde{\psi}_n \rangle + \sum_a \tilde{n}_c^a(\mathbf{r}), \quad (3.24)$$

$$n^a(\mathbf{r}) = \sum_{ij} D_{ji}^a \langle \phi_i^a | \mathbf{r} \rangle \langle \mathbf{r} | \phi_j^a \rangle + n_c^a(\mathbf{r}), \quad (3.25)$$

$$\tilde{n}^a(\mathbf{r}) = \sum_{ij} D_{ji}^a \langle \tilde{\phi}_i^a | \mathbf{r} \rangle \langle \mathbf{r} | \tilde{\phi}_j^a \rangle + \tilde{n}_c^a(\mathbf{r}). \quad (3.26)$$

To clarify the rationale for adding  $\tilde{n}_c^a(\mathbf{r})$ , consider that if we had *not* done so, any contribution of the all-electron core density outside the augmentation sphere would cause  $n^a(\mathbf{r})$  and  $\tilde{n}^a(\mathbf{r})$  to differ, which they are only allowed to do *within* the augmentation sphere. Since this is the *only* requirement, the part of  $\tilde{n}_c^a(\mathbf{r})$  inside can be chosen as we see fit, which means any smooth function. In GPAW, the pseudo core density is chosen to be a sixth order polynomial with only even powers, where the coefficients ensure that pseudo and all-electron core densities join each other smoothly (if uneven powers are included, the derivative of corresponding order will become discontinuous at  $r = 0$ ).

### 3.3.2 Coulomb interaction

The total Coulombic energy contribution is due to electronic and nuclear charges, where the electronic contribution  $n(\mathbf{r})$  has already been separated into smooth and atomic contributions as seen above. However the nuclear charges  $Z^a$  and core electron density still introduce sharp peaks in the electrostatic potential, which are detrimental to our efforts to have only smooth entities on our primary (real or reciprocal space) grids.

Let  $\rho(\mathbf{r})$  denote the total negative charge distribution:

$$\rho(\mathbf{r}) = n(\mathbf{r}) + \sum_a Z^a(\mathbf{r}) = n(\mathbf{r}) - \sum_a Z^a \delta(\mathbf{r} - \mathbf{R}^a), \quad (3.27)$$

which uses Dirac delta functions to express the nuclear point charges  $Z^a$ . We now introduce the *compensation charges*  $\tilde{Z}^a(\mathbf{r})$ , smooth charge distributions localized within the augmentation region of each atom. The compensation charges are defined to cancel out the Coulomb interaction from the augmentation regions (which can be accomplished by requiring them to have the same multipole expansion, see below), thereby making the radially represented charge density in the augmentation region neutral for the purposes of the regular-grid operations.

In order to save the rainforest we define the notation

$$(f|g) = \int \frac{f(\mathbf{r})g(\mathbf{r}')}{\|\mathbf{r} - \mathbf{r}'\|} d^3\mathbf{r} d^3\mathbf{r}', \quad (3.28)$$

and let  $((\rho)) = (\rho|\rho)$ . The Hartree energy of the total charge is then<sup>3</sup>

$$E_{\text{Ha}} = \frac{1}{2}((\rho)) = \frac{1}{2}(n + \sum_a Z^a). \quad (3.29)$$

Now, writing the nuclear charges as  $Z^a = \tilde{Z}^a + (Z^a - \tilde{Z}^a)$ , we can distribute the different terms in such a way that we achieve charge neutrality in each region:

$$\begin{aligned} ((\rho)) &= \left( \left( \tilde{n} + \sum_a \tilde{Z}^a + \sum_a (n^a - \tilde{n}^a + Z^a - \tilde{Z}^a) \right) \right) \\ &= \left( \left( \tilde{n} + \sum_a \tilde{Z}^a \right) \right) + \left( \left( \sum_a (n^a - \tilde{n}^a + Z^a - \tilde{Z}^a) \right) \right) \\ &\quad + 2 \sum_b \left( \tilde{n} + \sum_a \tilde{Z}^a \middle| n^b - \tilde{n}^b + Z^b - \tilde{Z}^b \right) \end{aligned} \quad (3.30)$$

<sup>3</sup>While this expression includes the infinite point charge self-interaction, this could be excluded at the cost of excessive notation. We shall keep these terms since they can be excluded at a later time.

The second and third terms can be simplified by noting that the cross-atom parts vanish, since  $n^a(\mathbf{r}) = \tilde{n}^a(\mathbf{r})$  and  $Z^a(\mathbf{r}) = \tilde{Z}^a(\mathbf{r})$  outside the augmentation sphere. Furthermore, using  $\tilde{n}(\mathbf{r}) = \tilde{n}^a(\mathbf{r})$  inside the augmentation region of atom  $a$ , we can get rid of  $\tilde{n}$  in the last term. Therefore

$$\begin{aligned}
((\rho)) &= ((\tilde{n} + \sum_a \tilde{Z}^a)) \\
&+ \sum_a \left\{ ((n^a + Z^a)) + ((\tilde{n}^a + \tilde{Z}^a)) - 2(n^a + Z^a | \tilde{n}^a + \tilde{Z}^a) \right\} \\
&+ 2 \sum_a \left\{ (n^a + Z^a | \tilde{n}^a + \tilde{Z}^a) - ((\tilde{n}^a + \tilde{Z}^a)) \right\} \\
&= ((\tilde{n} + \sum_a \tilde{Z}^a)) + \sum_a \left\{ ((n^a + Z^a)) - ((\tilde{n}^a + \tilde{Z}^a)) \right\} \\
&= ((\tilde{\rho})) + \sum_a \left\{ ((\rho^a)) - ((\tilde{\rho}^a)) \right\}, \tag{3.31}
\end{aligned}$$

where

$$\tilde{\rho}(\mathbf{r}) = \tilde{n}(\mathbf{r}) + \sum_a \tilde{Z}^a(\mathbf{r}), \tag{3.32}$$

$$\rho^a(\mathbf{r}) = n^a(\mathbf{r}) + Z^a(\mathbf{r}) = n^a(\mathbf{r}) - Z^a \delta(\mathbf{r} - \mathbf{R}^a), \tag{3.33}$$

$$\tilde{\rho}^a(\mathbf{r}) = \tilde{n}^a(\mathbf{r}) + \tilde{Z}^a(\mathbf{r}). \tag{3.34}$$

As mentioned before, the compensation charges are selected such that the multipole expansion of the charge on the radial grid is zero, to avoid interactions with charges outside the augmentation region. We use a circumflex to denote normalization ( $\hat{\mathbf{r}} = \mathbf{r}/r$ ). Now, if  $Y_{lm}(\hat{\mathbf{r}}) = Y_L(\hat{\mathbf{r}})$  are the spherical harmonics[21, p. 283], using  $L$  as a composite index for  $l$  and  $m$ , then the  $L$ 'th term of the multipole expansion reads

$$\begin{aligned}
0 &= \int \|\mathbf{r} - \mathbf{R}^a\|^l Y_L(\widehat{\mathbf{r} - \mathbf{R}^a}) \left[ n^a(\mathbf{r}) - \tilde{n}^a(\mathbf{r}) + Z^a(\mathbf{r}) - \tilde{Z}^a(\mathbf{r}) \right] d^3\mathbf{r} \\
&= \sum_{ij} \Delta_{Lij}^a D_{ji}^a + \Delta_{00}^a \delta_{0l} - \int \|\mathbf{r} - \mathbf{R}^a\|^l Y_L(\widehat{\mathbf{r} - \mathbf{R}^a}) \tilde{Z}^a(\mathbf{r}) d^3\mathbf{r}, \tag{3.35}
\end{aligned}$$

where we have used the atomic density definitions (3.25) and (3.26), remembering that the core state densities are radial with respect to  $\mathbf{r} - \mathbf{R}^a$ , to define

$$\Delta_{Lij}^a = \int \|\mathbf{r} - \mathbf{R}^a\|^l Y_L(\widehat{\mathbf{r} - \mathbf{R}^a}) \left[ \phi_i^a(\mathbf{r}) \phi_j^a(\mathbf{r}) - \tilde{\phi}_i^a(\mathbf{r}) \tilde{\phi}_j^a(\mathbf{r}) \right] d^3\mathbf{r}, \tag{3.36}$$

$$\Delta_{00}^a = \int Y_{00}(\hat{\mathbf{r}}) \left[ -Z^a \delta(\mathbf{r}) + n_c^a(r) - \tilde{n}_c^a(r) \right] d^3\mathbf{r}. \tag{3.37}$$

The spherical harmonics form a complete set, so we can expand<sup>4</sup> the compensation charges as

$$\tilde{Z}^a(\mathbf{r}) = \sum_L Q_L^a \tilde{g}_L^a(\mathbf{r}) = \sum_L Q_L^a \tilde{g}_L^a(\|\mathbf{r} - \mathbf{R}^a\|) Y_L(\widehat{\mathbf{r} - \mathbf{R}^a}), \tag{3.38}$$

<sup>4</sup>The sum is over all  $l = 0 \dots \infty$  and  $m = -l \dots l$ . In practice[10] we assume  $\infty \approx 2$ .

where  $\tilde{g}_l^a$  are normalized radial functions, which we choose to be Gaussians. We then use the orthogonality property of spherical harmonics to obtain from (3.35) an expression for the coefficients

$$Q_L^a = \sum_{ij} \Delta_{Lij}^a D_{ji}^a + \Delta_{00}^a \delta_{l0}. \quad (3.39)$$

Thus we have a final expression for the Hartree energy

$$E^{\text{Ha}}[\rho] = E^{\text{Ha}}[\tilde{\rho}] + \sum_a (E^{\text{Ha}}[\rho^a] - E^{\text{Ha}}[\tilde{\rho}^a]), \quad (3.40)$$

where the atomic contributions – again – depend only on the pseudo wave functions through the atomic density matrices  $D_{ij}^a$ , the remaining quantities being evaluated in the isolated-atom context.

### 3.3.3 Exchange-correlation functional

If the chosen exchange-correlation functional is (sufficiently) local, then

$$E_{\text{xc}}[n] = E_{\text{xc}}[\tilde{n}] + \sum_a (E_{\text{xc}}[n^a] - E_{\text{xc}}[\tilde{n}^a]), \quad (3.41)$$

since  $\tilde{n}(\mathbf{r}) = \tilde{n}^a(\mathbf{r})$  everywhere inside each augmentation sphere, while  $n(\mathbf{r}) = \tilde{n}(\mathbf{r})$  everywhere outside.

### 3.3.4 The zero potential

Both for the density and the compensation charges, we have added and subtracted quantities on the regular and radial grid to shift troublesome terms to more suitable places. We can also do this with any fictional atomic potential  $\bar{v}^a(\mathbf{r})$  which is localized to the augmentation region, as long as this potential is mirrored on the regular grid to compensate.

For the isolated atom, the pseudo charge density and pseudo exchange-correlation interaction correspond to a smooth potential contribution which will be “felt” by the wave functions on the regular grid during a calculation. We can choose the *zero potential*  $\bar{v}^a(\mathbf{r})$  to make this potential even more smooth. In GPAW, the zero potential is defined such that the atomic potential satisfies

$$v_{\text{atom}}(r) = v_{\text{Ha}}(r) + v_{\text{xc}}(r) + \bar{v}(r) = a + br^2 \quad (3.42)$$

within the augmentation region,  $a$  and  $b$  ensuring smoothness at the cutoff.

The energy contribution due to this potential is then

$$\int \tilde{n}(\mathbf{r}) \sum_a \bar{v}^a(\mathbf{r}) d^3\mathbf{r} - \sum_a \int \tilde{n}^a(\mathbf{r}) \bar{v}^a(\mathbf{r}) d^3\mathbf{r} \approx 0. \quad (3.43)$$

### 3.3.5 Total energy

Each of the troublesome quantities in the total energy expression (2.13) has now been reformulated in terms of smooth parts and parts which can be handled on radial grids. We can now collect the results in a final energy expression

$$E = \tilde{E} + \sum_a \Delta E^a = \tilde{E} + \sum_a (E^a - \tilde{E}^a), \quad (3.44)$$

where

$$\begin{aligned} \tilde{E} &= \sum_n f_n \langle \tilde{\psi}_n | -\frac{1}{2} \nabla^2 | \tilde{\psi}_n \rangle + \frac{1}{2} \int \frac{\tilde{\rho}(\mathbf{r}) \tilde{\rho}(\mathbf{r}')}{\|\mathbf{r} - \mathbf{r}'\|} d^3\mathbf{r} d^3\mathbf{r}' \\ &\quad + \int \tilde{n}(\mathbf{r}) \sum_a \bar{v}^a(\mathbf{r}) d^3\mathbf{r} + E_{\text{xc}}[\tilde{n}], \end{aligned} \quad (3.45)$$

$$\begin{aligned} E^a &= \sum_{ij} D_{ji}^a \langle \phi_i^a | -\frac{1}{2} \nabla^2 | \phi_j^a \rangle + \sum_c \langle \phi_c^a | -\frac{1}{2} \nabla^2 | \phi_c^a \rangle \\ &\quad + \frac{1}{2} \int \frac{\rho^a(\mathbf{r}) \rho^a(\mathbf{r}')}{\|\mathbf{r} - \mathbf{r}'\|} d^3\mathbf{r} d^3\mathbf{r}' + E_{\text{xc}}[n^a], \end{aligned} \quad (3.46)$$

$$\begin{aligned} \tilde{E}^a &= \sum_{ij} D_{ji}^a \langle \tilde{\phi}_i^a | -\frac{1}{2} \nabla^2 | \tilde{\phi}_j^a \rangle + \frac{1}{2} \int \frac{\tilde{\rho}^a(\mathbf{r}) \tilde{\rho}^a(\mathbf{r}')}{\|\mathbf{r} - \mathbf{r}'\|} d^3\mathbf{r} d^3\mathbf{r}' \\ &\quad + \int \tilde{n}^a(\mathbf{r}) \bar{v}^a(\mathbf{r}) d^3\mathbf{r} + E_{\text{xc}}[\tilde{n}^a]. \end{aligned} \quad (3.47)$$

Importantly, once again the atomic parts  $\Delta E^a = E^a - \tilde{E}^a$  depend on the pseudo wave functions *only* through  $D_{ij}^a$ .

### 3.4 The PAW Hamiltonian

For the purposes of the following partial derivatives, the following variables are considered distinct: the pseudo wave functions  $\tilde{\psi}_n(\mathbf{r})$ , the pseudo electron density  $\tilde{n}(\mathbf{r})$  and the atomic density matrices  $D_{ij}^a$ . There are *no* other variables which depend on  $\tilde{\psi}_n(\mathbf{r})$  in any of the energy expressions – for example the pseudo charge is  $\tilde{\rho} = \tilde{n} + \tilde{Z}^a$ , where the compensation charges depend only on  $D_{ij}^a$ .

We wish to define the pseudo Hamiltonian in a way similar to the ordinary Kohn-Sham Hamiltonian of Chapter 2, only this time in terms of a derivative with respect to the conjugate *pseudo* wave function, since we want these to be our variational parameters. Using the chain rule,

$$\frac{\delta E}{\delta \tilde{\psi}_n^*(\mathbf{r})} = \left. \frac{\delta E}{\delta \tilde{\psi}_n^*(\mathbf{r})} \right|_{\text{fix}} + \left. \frac{\delta E}{\delta \tilde{n}(\mathbf{r})} \right|_{\text{fix}} \frac{\delta \tilde{n}(\mathbf{r})}{\delta \tilde{\psi}_n^*(\mathbf{r})} + \sum_{aij} \left. \frac{\partial E}{\partial D_{ij}^a} \right|_{\text{fix}} \frac{\delta D_{ij}^a}{\delta \tilde{\psi}_n^*(\mathbf{r})}, \quad (3.48)$$

where the subscript *fix* denotes that the other variables are held constant, though after this warning we shall omit this notation. We will now consider each of the derivatives in turn. We define the *pseudo Hartree potential* as

$$\tilde{v}_{\text{Ha}}(\mathbf{r}) = \frac{\delta E}{\delta \tilde{\rho}(\mathbf{r})} = \frac{1}{2} \frac{\delta}{\delta \tilde{\rho}(\mathbf{r})} \int \frac{\tilde{\rho}(\mathbf{r}) \tilde{\rho}(\mathbf{r}')}{\|\mathbf{r} - \mathbf{r}'\|} d^3\mathbf{r} d^3\mathbf{r}' = \int \frac{\tilde{\rho}(\mathbf{r}')}{\|\mathbf{r} - \mathbf{r}'\|} d^3\mathbf{r}', \quad (3.49)$$

and the *pseudo effective potential* as

$$\begin{aligned} \tilde{v}_{\text{eff}}(\mathbf{r}) &= \frac{\delta E}{\delta \tilde{n}(\mathbf{r})} = \frac{\delta E_{\text{Ha}}[\tilde{\rho}]}{\delta \tilde{\rho}(\mathbf{r})} \frac{\delta \tilde{\rho}(\mathbf{r})}{\delta \tilde{n}(\mathbf{r})} + \sum_a \bar{v}^a(\mathbf{r}) + \frac{\delta E_{\text{xc}}[\tilde{n}]}{\delta \tilde{n}(\mathbf{r})} \\ &= \tilde{v}_{\text{Ha}}(\mathbf{r}) + \sum_a \bar{v}^a(\mathbf{r}) + \tilde{v}_{\text{xc}}(\mathbf{r}), \end{aligned} \quad (3.50)$$

where we have also defined the pseudo exchange-correlation potential  $\tilde{v}_{\text{xc}}(\mathbf{r}) = \frac{\delta E_{\text{xc}}[\tilde{n}]}{\delta \tilde{n}(\mathbf{r})}$ . Next, the derivative of the density is simply

$$\frac{\delta \tilde{n}(\mathbf{r})}{\delta \tilde{\psi}_n^*(\mathbf{r})} = f_n \tilde{\psi}_n(\mathbf{r}), \quad (3.51)$$

and for the atomic density matrices we have

$$\begin{aligned} \frac{\delta D_{ij}^a}{\delta \tilde{\psi}_n^*(\mathbf{r})} &= \frac{\delta}{\delta \tilde{\psi}_n^*(\mathbf{r})} \sum_{n'} \int f_{n'} \langle \tilde{p}_i^a | \tilde{\psi}_{n'} \rangle \tilde{\psi}_{n'}^*(\mathbf{r}') \tilde{p}_j^a(\mathbf{r}') d^3 \mathbf{r}' \\ &= f_n \tilde{p}_j^a(\mathbf{r}) \langle \tilde{p}_i^a | \tilde{\psi}_n \rangle. \end{aligned} \quad (3.52)$$

Last, define the *atomic Hamiltonians* as

$$\begin{aligned} \Delta H_{ji}^a &= \frac{\partial E}{\partial D_{ij}^a} = \frac{\partial \tilde{E}}{\partial D_{ij}^a} + \frac{\partial \Delta E^a}{\partial D_{ij}^a}, \\ \frac{\partial \tilde{E}}{\partial D_{ij}^a} &= \int \frac{\delta \tilde{E}}{\delta \tilde{\rho}(\mathbf{r})} \sum_L \frac{\partial \tilde{\rho}(\mathbf{r})}{\partial Q_L^a} \frac{\partial Q_L^a}{\partial D_{ij}^a} d^3 \mathbf{r} = \int \tilde{v}_{\text{Ha}}(\mathbf{r}) \sum_L \Delta_{Lij}^a \tilde{g}_L^a(\mathbf{r}) d^3 \mathbf{r}. \end{aligned} \quad (3.53)$$

Explicit evaluation of  $\frac{\partial \Delta E^a}{\partial D_{ij}^a}$  is omitted since it suffices to note that it is a function of  $D_{ij}^a$  and large numbers of isolated-atom variables[10, App. D]. The energy derivative then becomes

$$\frac{\delta E}{\delta \tilde{\psi}_n^*(\mathbf{r})} = -\frac{1}{2} f_n \nabla^2 \tilde{\psi}_n(\mathbf{r}) + f_n \tilde{v}_{\text{eff}}(\mathbf{r}) \tilde{\psi}_n(\mathbf{r}) + f_n \sum_{aij} \tilde{p}_j^a(\mathbf{r}) \Delta H_{ji}^a \langle \tilde{p}_i^a | \tilde{\psi}_n \rangle, \quad (3.54)$$

which is equal to  $f_n \hat{H} \tilde{\psi}_n(\mathbf{r})$  cf. (2.14) if and only if the pseudo Hamiltonian is

$$\hat{H} = -\frac{1}{2} \nabla^2 + \tilde{v}_{\text{eff}} + \sum_{aij} |\tilde{p}_i^a\rangle \Delta H_{ij}^a \langle \tilde{p}_j^a|. \quad (3.55)$$

The pseudo Hamiltonian thus consists of the usual kinetic energy operator, the somewhat modified effective potential and a new, non-local atomic term which is specific to the PAW method.

### 3.5 Modified variational problem

Applying the transformation  $\hat{\mathcal{T}}$ , we can rewrite the variational problem (2.15) in terms of pseudo wave functions:

$$\Omega = E[\{\psi_n\}] - \sum_{mn} \lambda_{mn} (\langle \psi_n | \psi_m \rangle - \delta_{nm}) \quad (3.56)$$

$$= E[\{\hat{\mathcal{T}} \tilde{\psi}_n\}] - \sum_{mn} \lambda_{mn} \left( \langle \tilde{\psi}_n | \hat{\mathcal{T}}^\dagger \hat{\mathcal{T}} | \tilde{\psi}_m \rangle - \delta_{nm} \right). \quad (3.57)$$

Importantly, this means the pseudo wave functions are no longer orthogonal, but instead must obey the special orthogonality condition

$$\langle \tilde{\psi}_n | \hat{\mathcal{T}}^\dagger \hat{\mathcal{T}} | \tilde{\psi}_m \rangle = \langle \tilde{\psi}_n | \hat{S} | \tilde{\psi}_m \rangle = \delta_{nm}. \quad (3.58)$$

The operator  $\hat{S}$  is the PAW transformation of the unit operator. The form of  $\hat{S}$  can be evaluated by substituting the unit operator for  $\hat{A}$  in the equation (3.19) for the expectation value and requiring the resulting relation to be true for all wave functions and occupation numbers. This yields

$$\hat{S} = 1 + \sum_{aij} |\tilde{p}_i^a\rangle \left( \langle \phi_i^a | \phi_j^a \rangle - \langle \tilde{\phi}_i^a | \tilde{\phi}_j^a \rangle \right) \langle \tilde{p}_j^a | = 1 + \sum_{aij} |\tilde{p}_i^a\rangle \Delta S_{ij}^a \langle \tilde{p}_j^a|. \quad (3.59)$$

Now set the derivative of the variational expression to zero:

$$0 = \frac{\delta \Omega}{\delta \tilde{\psi}_n^*(\mathbf{r})} = \frac{\delta E}{\delta \tilde{\psi}_n^*(\mathbf{r})} - \sum_m \lambda_{mn} \hat{S} \tilde{\psi}_m(\mathbf{r}), \quad (3.60)$$

yielding the general expression

$$f_n \hat{H} |\tilde{\psi}_n\rangle = \sum_m \lambda_{mn} \hat{S} |\tilde{\psi}_m\rangle, \quad (3.61)$$

where the states are not generally eigenvectors. The final form of the Kohn-Sham equations corresponding to a diagonalized Lagrange multiplier matrix is (cf. Section 2.3)

$$\hat{H} |\tilde{\psi}_n\rangle = \epsilon_n \hat{S} |\tilde{\psi}_n\rangle. \quad (3.62)$$

This completes our description of the PAW formalism. The iterative scheme outlined in Section 2.4 is used to obtain the eigenstates. During an iterative solution, it is – aside from the operations already listed in the Kohn-Sham solution scheme – also necessary to evaluate the inner products between pseudo wave functions and projectors. Aside from this, the atomic variables can be precalculated. An element-specific collection containing all the required atomic quantities, such as projectors, partial waves, zero potential, core densities, atomic kinetic energy contributions and so on are called *PAW setups*.

Smoothness of the pseudo wave functions and other regular-grid based quantities allows for surprisingly coarse grid resolutions. In GPAW, wave function grid spacings of around 0.15 to 0.2 Å are generally sufficient to obtain well-converged results. Some quantities, such as the Hartree potential, are represented on finer grids (generally half the grid spacing). The most important approximations pertaining to the PAW method are finite grid spacing, projector/partial wave completeness and the frozen core approximation.

The next chapter deals with the use of localized basis functions to represent the wave functions. The primary difference is that many operators will be represented by matrices whose elements take the form of two-center integrals, but the results of this chapter are generally still valid down to a few substitutions.





# Chapter 4

## Atomic basis sets

So far we have considered the PAW formalism mainly in terms of real-space grid-based wave functions. This chapter describes the transition from grid-based calculations to the use of localized basis functions, focusing on general issues pertaining to the *calculations*, while the *generation* of basis sets will be the subject of the following chapter.

### 4.1 Background

DFT codes which use plane-wave or real-space grid basis sets have the ability to represent any wave function with arbitrary precision given sufficiently fine grids.

The use of small, exclusive sets of basis functions allows calculation time and memory requirements to be reduced considerably at the cost of accuracy. In a small basis set, the individual functions must be chosen carefully. Multiple different schemes have been devised to accommodate reasonably accurate representations using small basis sets.

- Linear combinations of Gaussian-type orbitals (GTOs) are widely used, since many expressions can then be evaluated analytically. The GAUSSIAN code, for example, uses GTOs.[28]
- Another possible choice is *Slater-type* orbitals (STOs), which have the form  $r^l e^{-\zeta r}$ , resembling simple orbitals. In Gaussian-based methods it is common to approximate STOs with fixed linear combinations of Gaussians to obtain a more orbital-like behaviour.
- *Numerical atomic orbitals* (NAOs) differ in that they are represented numerically on radial grids rather than analytically. While this makes calculations more time consuming, many of the required radial integrations can be performed beforehand and tabulated. NAOs have the advantage that they can be designed with any shape without extra computational cost, and can easily be localized to avoid expensive long-range interactions, thus achieving better scaling.
- Our approach is to use a basis of localized *pseudo atomic orbitals* (PAOs), which are simply NAOs adapted to the use of pseudopotentials or, in the

present case, the PAW method. This is quite similar to the approach in SIESTA, although the formalism is somewhat different.

In many cases these limited basis sets are chosen to be atom-centered orbitals, though they could equally well be located elsewhere.

## 4.2 Localized functions

What we are about to introduce is an expansion

$$|\tilde{\psi}_n\rangle = \sum_{\mu} c_{\mu n} |\Phi_{\mu}\rangle \quad (4.1)$$

of the pseudo wave functions  $|\tilde{\psi}_n\rangle$  in terms of localized atom-centered orbital-like functions  $|\Phi_{\mu}\rangle$ . While so far the variational parameters have been the real-space grid representations of the pseudo wave functions, it will now be the set of coefficients  $c_{\mu n}$ . This will have roughly the following consequences:

- The variational problem must be reformulated in terms of coefficients. The small number of parameters allows for a full diagonalization to be performed in every self-consistency iteration (cf. Section 2.4).
- Grid-based inner products such as  $\langle \tilde{\psi}_n | -\frac{1}{2}\nabla^2 | \tilde{\psi}_n \rangle$  or  $\langle \tilde{p}_i^a | \tilde{\psi}_n \rangle$  will be replaced by linear combinations of *two-center integrals*, which are taken care of differently.

Basis functions, projectors and several other entities are compactly supported functions defined on real space, each being centered on an atom. Generally, each such function is represented as an arbitrary radial part times an angular part, which is a spherical harmonic function. Implementation-wise, the radial parts are stored as splines on a one-dimensional grid whereas, as we shall see, the spherical harmonics can be accounted for analytically. For any such function  $X$  on any atom  $a$  we may write

$$X(\mathbf{r} - \mathbf{R}^a) = X(\mathbf{r}^a) = \chi(r^a) Y_{lm}(\hat{\mathbf{r}}^a), \quad (4.2)$$

where  $\mathbf{r}^a = \mathbf{r} - \mathbf{R}^a$  are nucleus-centered coordinates.

## 4.3 Two-center integrals

Inner products between localized functions appear in several places, most notably the total energy expression. It is for this reason necessary to calculate the product integral of two localized functions  $\Phi(\mathbf{r})$  and  $X(\mathbf{r})$ . In all relevant cases, one of the functions is a basis function whereas the other is either a basis function, the Laplacian of a basis function, or a projector function. Let the functions be centered on atoms  $a$  and  $b$  with coordinates  $\mathbf{R}^a$  and  $\mathbf{R}^b$ , where  $a$  and  $b$  are probably distinct:

$$\Phi(\mathbf{r}^a) = \varphi(r^a) Y_{L_1}(\hat{\mathbf{r}}^a), \quad (4.3)$$

$$X(\mathbf{r}^b) = \chi(r^b) Y_{L_2}(\hat{\mathbf{r}}^b). \quad (4.4)$$

The overlap integral  $\langle \Phi | X \rangle$  is nominally a function of both nuclear coordinates  $\mathbf{R}^a$  and  $\mathbf{R}^b$ , though clearly, since the overlap is translation invariant, it depends only on the atomic separation vector  $\mathbf{R}^b - \mathbf{R}^a$ :

$$\langle \Phi | X \rangle = \int \Phi^*(\mathbf{r} - \mathbf{R}^a) X(\mathbf{r} - \mathbf{R}^b) d^3\mathbf{r} = \int \Phi^*(\mathbf{r}) X(\mathbf{r} - \mathbf{R}^b + \mathbf{R}^a) d^3\mathbf{r}, \quad (4.5)$$

for which reason it suffices to describe it by the function

$$\Theta(\mathbf{R}) = \int \Phi^*(\mathbf{r}) X(\mathbf{r} - \mathbf{R}) d^3\mathbf{r}. \quad (4.6)$$

This inner product is calculated using the same method as in SIESTA. We shall not describe this in detail (for a more detailed description, see the thesis by Marco Vanin[17]), but will simply note the most important features since we will need the final form in Chapter 7. This method uses the convolution theorem of Fourier transforms to reexpress the overlap (4.6) in terms of the Fourier transformed functions  $\Phi^*(\mathbf{q})$  and  $X(\mathbf{q})$ , such that

$$\Theta(\mathbf{R}) = \int \Phi^*(\mathbf{q}) X(\mathbf{q}) e^{-i\mathbf{q}\cdot\mathbf{R}} d^3\mathbf{q}. \quad (4.7)$$

By expanding the exponential in spherical harmonics, the overlap expression can be reduced to a linear combination of spherical harmonics

$$\Theta(\mathbf{R}) = \langle \Phi | X \rangle = \sum_L \Theta_L(R) Y_L(\hat{\mathbf{R}}). \quad (4.8)$$

The radial functions  $\Theta_L(R)$  are evaluated by means of a Fourier-space integral, and each of them can be represented by a spline. Note that if multiple localized functions with identical shapes appear reside on different atoms, they are still described by the same splines, thus saving Fourier transforms.

For future benefit we define the *kinetic energy overlap matrix*  $T_{\mu\nu}$ , the *projector overlap matrix*<sup>1</sup>  $P_{i\mu}$  and the *basis function overlap matrix*  $S_{\mu\nu}$

$$T_{\mu\nu} = \langle \Phi_\mu | -\frac{1}{2}\nabla^2 | \Phi_\nu \rangle, \quad (4.9)$$

$$P_{i\mu}^a = \langle \tilde{p}_i^a | \Phi_\mu \rangle, \quad (4.10)$$

$$S_{\mu\nu} = \langle \Phi_\mu | \hat{S} | \Phi_\nu \rangle = \langle \Phi_\mu | \Phi_\nu \rangle + \sum_{aij} \langle \Phi_\mu | \tilde{p}_i^a \rangle \Delta S_{ij} \langle \tilde{p}_j^a | \Phi_\nu \rangle. \quad (4.11)$$

These overlaps can be evaluated once the atomic positions are known by calling the relevant splines with the relevant atomic separation vector. In the case where the overlap involves a Laplacian, the Fourier transform differentiation trick

$$\int_{-\infty}^{\infty} \frac{df(x)}{dx} e^{iqx} dt = iq \int_{-\infty}^{\infty} f(x) e^{iqx} dt \quad (4.12)$$

is used rather than explicitly evaluating the Laplacian of the function.

<sup>1</sup>Note that the variable  $P_{ni}^a$  in the original GPAW article[10] corresponds to the adjoint of this matrix judging by the order of the indices, but the present convention is chosen to ensure that all the overlap matrices have the usual antilinear/linear behaviour.

## 4.4 Matrix formulation

Once again we want to formulate a Hamiltonian in terms of a derivative of the energy.<sup>2</sup> First of all, this requires an expression for the energy, which will now involve various two-center integrals. Second, since we no longer can use the pseudo wave functions themselves as parameters, we will have to reformulate the variational problem again, obtaining a matrix form of the Kohn-Sham equations.

We consider again the pseudo wave function expansion

$$|\tilde{\psi}_n\rangle = \sum_{\mu} c_{\mu n} |\Phi_{\mu}\rangle. \quad (4.13)$$

The matrix of expansion coefficients  $\mathbf{C} = [c_{\mu n}]$  describes the transformation between the pseudo wave functions and the basis functions, although it does not technically represent a change of basis since it is not generally a square matrix.<sup>3</sup> Now, for any operator  $\hat{A}$ , we may write

$$\langle \tilde{\psi}_n | \hat{A} | \tilde{\psi}_m \rangle = \sum_{\mu\nu} c_{\mu n}^* \langle \Phi_{\mu} | \hat{A} | \Phi_{\nu} \rangle c_{\nu m}, \quad (4.14)$$

which in matrix notation becomes the familiar-looking

$$\mathbf{A}' = \mathbf{C}^{\dagger} \mathbf{A} \mathbf{C}, \quad (\mathbf{A})_{\mu\nu} = \langle \Phi_{\mu} | \hat{A} | \Phi_{\nu} \rangle, \quad (\mathbf{A}')_{mn} = \langle \tilde{\psi}_m | \hat{A} | \tilde{\psi}_n \rangle. \quad (4.15)$$

Specifically, the pseudo wave function orthogonality condition becomes

$$\langle \tilde{\psi}_m | \hat{S} | \tilde{\psi}_n \rangle = \sum_{\mu\nu} c_{\mu m}^* \langle \Phi_{\mu} | \hat{S} | \Phi_{\nu} \rangle c_{\nu n} = \delta_{mn} \quad (4.16)$$

or

$$\mathbf{C}^{\dagger} \mathbf{S} \mathbf{C} = \mathbf{I}, \quad S_{\mu\nu} = \langle \Phi_{\mu} | \hat{S} | \Phi_{\nu} \rangle. \quad (4.17)$$

Let  $\mathbf{F} = \text{diag}(\{f_n\})$  be the diagonal matrix of occupation numbers  $f_n$  and define

$$\boldsymbol{\rho} = \mathbf{C} \mathbf{F} \mathbf{C}^{\dagger}, \quad \rho_{\mu\nu} = \sum_n c_{\mu n} f_n c_{\nu n}^*. \quad (4.18)$$

This operator will prove quite useful because, as we will see, the energy depends on coefficients and occupation numbers *only* through  $\rho_{\mu\nu}$ . Observe that for any operator  $\hat{A}$ ,

$$\begin{aligned} \sum_n f_n \langle \tilde{\psi}_n | \hat{A} | \tilde{\psi}_n \rangle &= \sum_{n\mu\nu} f_n c_{n\mu}^* \langle \Phi_{\mu} | \hat{A} | \Phi_{\nu} \rangle c_{n\nu} = \sum_{\mu\nu} \rho_{\nu\mu} \langle \Phi_{\mu} | \hat{A} | \Phi_{\nu} \rangle \\ &= \text{Tr}[\boldsymbol{\rho} \mathbf{A}], \end{aligned} \quad (4.19)$$

<sup>2</sup>Calculating the matrix elements  $\langle \Phi_{\mu} | \hat{H} | \Phi_{\nu} \rangle$  of the PAW Hamiltonian (3.55) directly would in fact yield the same result with less work, but having a relation which directly connects an energy derivative with the Hamiltonian will prove useful e.g. for force calculations. In fact, the reason for providing such detailed commentary on this relatively simple transformation is that we will need all the equations when calculating forces.

<sup>3</sup>In practice some circumstances, such as matrix diagonalization, prompt the adoption of square matrices. The number of Kohn-Sham states is then increased to the number of atomic orbitals for the purposes of these operations, while the extraneous columns are discarded afterwards.

i.e.  $\rho$  represents the state operator except it does not include any atomic or core state contributions. A more correct name would therefore be the *pseudo valence Kohn-Sham state operator*, though it shall henceforth be known as just the *state operator*. The pseudo kinetic energy can then be rewritten as

$$\sum_n f_n \langle \tilde{\psi}_n | -\frac{1}{2} \nabla^2 | \tilde{\psi}_n \rangle = \sum_{n\mu\nu} f_n c_{\mu n}^* \langle \Phi_\mu | -\frac{1}{2} \nabla^2 | \Phi_\nu \rangle c_{\nu n} = \sum_{\mu\nu} T_{\mu\nu} \rho_{\nu\mu}, \quad (4.20)$$

the pseudo electron density is

$$\tilde{n}(\mathbf{r}) = \sum_n f_n \tilde{\psi}_n^*(\mathbf{r}) \tilde{\psi}_n(\mathbf{r}) + \sum_a \tilde{n}_c^a(\mathbf{r}) = \sum_{\mu\nu} \rho_{\nu\mu} \Phi_\mu^*(\mathbf{r}) \Phi_\nu(\mathbf{r}) + \sum_a \tilde{n}_c^a(\mathbf{r}), \quad (4.21)$$

and the atomic density matrices are

$$D_{ij}^a = \sum_{n\mu\nu} f_n c_{\nu n} \langle \tilde{p}_i^a | \Phi_\nu \rangle \langle \Phi_\mu | \tilde{p}_j^a \rangle c_{\mu n}^* = \sum_{\mu\nu} P_{i\nu} \rho_{\nu\mu} P_{j\mu}^*. \quad (4.22)$$

These are of course trivial observations, but one *important* difference from previous cases is that the quantities, at least except the density, are now given in terms of the two-center integrals introduced in the previous section. Also, this means that all wave function dependent quantities in the energy expression (3.44) can be expressed purely by the state operator, and we may consequently define the Hamiltonian as a matrix such that each of its elements corresponds to the derivative of the energy with respect to a matrix element of the state operator:

$$\begin{aligned} \frac{\partial E}{\partial \rho_{\nu\mu}} &= T_{\mu\nu} + \int \frac{\delta E}{\delta \tilde{n}(\mathbf{r})} \frac{\partial \tilde{n}(\mathbf{r})}{\partial \rho_{\nu\mu}} d^3\mathbf{r} + \sum_{aij} \frac{\partial E}{\partial D_{ij}^a} \frac{\partial D_{ij}^a}{\partial \rho_{\nu\mu}} \\ &= T_{\mu\nu} + \int \Phi_\mu^*(\mathbf{r}) \tilde{v}_{\text{eff}}(\mathbf{r}) \Phi_\nu(\mathbf{r}) d^3\mathbf{r} + \sum_{aij} P_{j\mu}^{a*} \Delta H_{ji}^a P_{i\nu}^a, \end{aligned} \quad (4.23)$$

prompting the definition of the *Hamiltonian matrix* as

$$H_{\mu\nu} = \frac{\partial E}{\partial \rho_{\nu\mu}} = T_{\mu\nu} + V_{\mu\nu} + \sum_{aij} P_{i\mu}^{a*} \Delta H_{ij}^a P_{j\nu}^a = \langle \Phi_\mu | \hat{H} | \Phi_\nu \rangle, \quad (4.24)$$

with the new *effective potential matrix*

$$V_{\mu\nu} = \langle \Phi_\mu | \tilde{v}_{\text{eff}} | \Phi_\nu \rangle. \quad (4.25)$$

The Hamiltonian matrix is straightforwardly the matrix representation of the ordinary PAW Hamiltonian (3.55). The effective potential matrix elements are evaluated by grid-based integrations, whereas the remaining basis function dependent entities  $T_{\mu\nu}$  and  $P_{i\mu}$  are two-center integrals. When calculating  $V_{\mu\nu}$ , if the cell is periodic and the calculation pertains to a particular  $k$ -point, the basis functions must be replaced by the corresponding Bloch states, and summed over all the cells they overlap with appropriate phases.

## 4.5 Variational problem

We can now write down our variational problem by exploiting the dependence of the energy on the state operator, and remembering the orthogonality condition (4.16):

$$\Omega = E(\rho) - \sum_{mn\mu\nu} \lambda_{nm} \left( c_{\mu m}^* \langle \Phi_\mu | \hat{S} | \Phi_\nu \rangle c_{\nu n} - \delta_{nm} \right). \quad (4.26)$$

The minimal energy occurs at a point where the energy is stationary with respect to the coefficients  $\{c_{\mu m}\}$ . By differentiation with respect to the conjugate coefficient  $c_{\xi k}^*$ , we get

$$\begin{aligned} \frac{\partial \Omega}{\partial c_{\xi k}^*} &= \sum_{\mu\nu} \frac{\partial E}{\partial \rho_{\mu\nu}} \frac{\partial \rho_{\mu\nu}}{\partial c_{\xi k}^*} \\ &\quad - \sum_{mn\mu\nu} \lambda_{nm} \left( \frac{\partial c_{\mu m}^*}{\partial c_{\xi k}^*} c_{\nu n} + c_{\mu m}^* \frac{\partial c_{\nu n}}{\partial c_{\xi k}^*} \right) \langle \Phi_\mu | \hat{S} | \Phi_\nu \rangle = 0. \end{aligned} \quad (4.27)$$

Observe that  $\frac{\partial c_{\nu n}^*}{\partial c_{\xi k}^*} = \delta_{\nu\xi} \delta_{nk}$ , whereas  $\frac{\partial c_{\mu n}}{\partial c_{\xi k}^*} = 0$ . Then if the electronic temperature is 0, such that the occupation numbers are fixed, we have

$$\frac{\partial \rho_{\mu\nu}}{\partial c_{\xi k}^*} = \sum_n \left( \frac{\partial c_{\mu n}}{\partial c_{\xi k}^*} c_{\nu n}^* + c_{\mu n} \frac{\partial c_{\nu n}^*}{\partial c_{\xi k}^*} \right) f_n = \delta_{\nu\xi} c_{\mu k} f_k. \quad (4.28)$$

Thereby (4.27) becomes

$$0 = \frac{\partial \Omega}{\partial c_{\xi k}^*} = \sum_{\mu} H_{\xi\mu} c_{\mu k} f_k - \sum_{n\nu} \langle \Phi_\xi | \hat{S} | \Phi_\nu \rangle c_{\nu n} \lambda_{nk}. \quad (4.29)$$

Finally we obtain the equation

$$\sum_{\mu} H_{\xi\mu} c_{\mu k} f_k = \sum_{n\nu} S_{\xi\nu} c_{\nu n} \lambda_{nk}, \quad (4.30)$$

either side of which is seen to be the  $(\xi, k)$ 'th element of a matrix product. Since this is supposed to be the case for all  $(\xi, k)$ , we can reformulate it in matrix notation as a generalized eigenvalue problem

$$\mathbf{HC} = \mathbf{SC}\mathbf{\Lambda}. \quad (4.31)$$

Here we have again taken the liberty of including the occupation numbers into the Lagrange multipliers, such that with diagonalization of  $\mathbf{\Lambda}$ , the Lagrange multipliers correspond to Kohn-Sham eigenenergies  $\mathbf{\Lambda} = \text{diag}\{\{\epsilon_n\}\}$ .

For completeness we shall mention that if we had differentiated by  $c_{\mu k}$  rather than  $c_{\mu k}^*$ , the result would have been the ‘‘adjoint’’ equation  $\mathbf{C}^\dagger \mathbf{H} = \mathbf{\Lambda} \mathbf{C}^\dagger \mathbf{S}$ , which is completely equivalent to (4.31) for real  $\mathbf{H}$ ,  $\mathbf{S}$  and  $\mathbf{\Lambda}$ . If all variables are assumed real, the result (4.31) is also obtained. This matrix problem is then solved during each self-consistency iteration, which is since the matrices involve only a small number of elements, at least compared to the grid-based wave functions which have degrees of freedom for each grid point. We now have a fully operational scheme for doing PAW calculations with atomic orbital basis sets. The next chapter concerns the choice and generation of basis functions to be used with this scheme.

# Chapter 5

## Basis set generation

In this chapter we shall describe the relevant types of basis functions and the process by which they are generated.

### 5.1 Overview of atomic basis sets

As mentioned previously, atomic orbitals are natural choices for atom-centered basis functions. These can readily be obtained from the single-particle all-electron wave functions which emerge from the solution of the Kohn-Sham equations for the isolated atom.<sup>1</sup>

However, the all-electron orbital is not well suited to represent the smooth extended wave functions prevalent in the PAW method. For this reason it will obviously be necessary to transform them into smooth *pseudo* atomic orbitals. Second, these orbitals are infinitely extended, which is of course unacceptable. One solution is to neglect any sufficiently small overlaps between orbitals, but it is generally better to make sure that the orbitals are strictly localized.<sup>2</sup> This we will achieve by adding a suitable external potential when solving the radial Kohn-Sham equations.

Since we are using the frozen core approximation, only valence states are of any interest. This means that so far, each element has a pseudo atomic orbital  $\Phi_{nlm}^{\text{PAO}}$  for every atomic valence state labelled by the principal, angular momentum and magnetic quantum numbers  $n$ ,  $l$  and  $m$ , given by

$$\Phi_{nlm}^{\text{PAO}}(\mathbf{r}) = \varphi_{nl}(r)Y_{lm}(\hat{\mathbf{r}}), \quad (5.1)$$

each of the orbitals being the product of a radial part  $\varphi_{ln}(r)$  which is independent of  $m$ , and a corresponding spherical harmonic.

The atomic orbitals themselves are typically not sufficient to achieve desirable accuracy. For this reason, extra radial functions are usually added to the atomic basis for each valence state with corresponding angular behaviour.

---

<sup>1</sup>A radial atomic Kohn-Sham solver is already implemented in GPAW since it is used to calculate the all-electron partial waves. This will be reused with certain modifications, as we shall see later.

<sup>2</sup>E. Artacho et al.[15] note that neglecting overlaps below a certain threshold rather than enforcing localization, while useful particularly for e.g. Gaussian-type orbitals, can lead to numerical instabilities due to the basis spanning a different Hilbert space.

Furthermore, while the isolated atoms possess valence states corresponding only to certain angular momentum quantum numbers  $l$ , thus allowing wave functions with only a certain angular behaviour, this restriction does not apply for systems other than the isolated atom. Therefore *polarization functions*, i.e. basis functions that correspond to values of  $l$  which do *not* appear on the isolated atom, can be used to improve the angular flexibility of the basis. In this case, one can also add extra radial functions for the same  $l$ , or include further polarization functions with even higher  $l$ , though with  $2l + 1$  different angular parts, this becomes increasingly expensive.

Depending on the number of radial functions per valence state and the number of polarization functions, we will refer to basis sets as “SZ” (single-zeta, containing atomic orbitals only), “DZP” (double-zeta polarized), “TZDP” (triple-zeta doubly-polarized) and so on.<sup>3</sup> Soler et al. note that DZP basis sets achieve good accuracy in SIESTA while still being computationally inexpensive, for which reason we shall aim primarily towards obtaining good basis sets of this kind.[11]

The following sections will describe in turn pseudo-atomic orbital calculation, multiple-zeta functions and polarization functions.

## 5.2 Atomic orbital calculation

Consider the Kohn-Sham equation<sup>4</sup> for some all-electron wave function  $X(\mathbf{r})$  on an isolated atom,

$$\left[ -\frac{1}{2}\nabla^2 + v_{\text{eff}}(r) \right] X(\mathbf{r}) = \epsilon X(\mathbf{r}), \quad (5.2)$$

where the effective potential is a purely radial function. This is a second-order linear partial differential equation which is separable into radial and angular parts. Let us define the trial product solution

$$X_{lnm}(\mathbf{r}) = \frac{\chi_{ln}(r)}{r} Y_{lm}(\hat{\mathbf{r}}), \quad (5.3)$$

where we have taken the liberty of naming the angular part and the indices in a rather suggestive manner, and we have extracted a factor of  $r$  in the radial part for future convenience. Plugging the trial solution into (5.2), using the spherical expression for the Laplacian, and dividing by  $X_{lnm}$ , one can readily show that radial as well as angular parts must each obey different differential equations (the method is described in e.g. [23]). For the angular part this results in spherical harmonic solutions which are eigenfunctions of the Laplacian, and the quantum numbers  $l$  and  $m$  emerge naturally.

The radial functions  $\chi_{ln}$ , being cause for more trouble, are determined by

$$-\frac{d^2\chi_{ln}(r)}{dr^2} + \left[ \frac{l(l+1)}{r^2} + 2(v_{\text{eff}}(r) - \epsilon_n) \right] \chi_{ln}(r) = 0, \quad (5.4)$$

<sup>3</sup>The name *zeta* probably stems from the letter  $\zeta$  being used to denote the decay parameter of Slater-type orbitals. Having several different Slater functions with different decay rates thus implies several “zetas”.

<sup>4</sup>Basis functions are so far calculated using the non-scalar-relativistic Kohn-Sham equations mentioned here, but it is possible to run the calculations with scalar-relativistic corrections too. This is relevant only for heavy elements.



with the boundary condition that the wave function must tend to zero at  $r \rightarrow \infty$  and at  $r = 0$  (since we are solving for  $rX(\mathbf{r})$ , this is true for s-type orbitals as well).

Since the all-electron wave functions oscillate rapidly near  $r = 0$ , it is advantageous to use a non-equidistant grid

$$r = \frac{\beta g}{N - g}, \quad g = 0 \dots N - 1, \quad (5.5)$$

$$g = \frac{rN}{\beta + r}. \quad (5.6)$$

This change of variables evidently alters the differential quotients in (5.4), though we shall not bother with these details. The differential equation is then solved numerically by guessing an energy, then integrating radially. In fact, one radial integration is performed from zero to a point somewhere in the middle, while another integration is performed backwards from infinity, technically meaning the outermost grid point. The two half-solutions are then joined in the middle. If the energy guess is wrong, these solutions cannot be joined differentiably, and the size of the derivative discontinuity can be used to adjust the energy guess. The procedure is repeated until the entire augmented solution is differentiable.

We use the PBE functional for exchange and correlation by default, since this is the most likely choice for serious calculations using the basis functions. It should also be noted that the solution is spin-paired.

Figure 5.1 shows all the all-electron Kohn-Sham wave functions for copper calculated using the above method. It will prove useful to note here that the radial part has an  $r^l$  asymptotical behaviour near  $r = 0$ .

### 5.2.1 Confinement scheme

The wave-function tails, being very large, are badly suited to numerical calculations. A simple way to obtain a wave function which is strictly confined to a small, finite region, is to place the atom in an infinite spherical potential well with some cutoff  $r_{\text{conf}}$ , which is equivalent to moving the boundary condition  $\chi = 0$  from infinity to  $r_{\text{conf}}$ .

Doing this we can simply use the solution method from above to obtain localized wave functions. However, a sudden jump in the potential to infinity generally implies a discontinuity in the first derivative of the wave functions at the boundary. Figure 5.2, shows the *free-atom* solution and a confined orbital using the *infinite* hard-wall potential. The discontinuity of the derivative will cause the second-order derivative to be infinite (or at least very high in grid-based terms), which yields unwanted contributions to the kinetic energy which might e.g. induce a considerable *egg-box effect* (a numerical error related to the inhomogeneity of space when using finite grid resolution; this is explained in Section 7.5). To prevent this, the wave function can be confined in a more controlled manner by adding an external confinement potential  $V_{\text{conf}}$  which is zero or close to zero near to the atom, but approaches infinity at the cutoff  $r_{\text{conf}}$ .

Specifically, we define the confinement potential in the same way as Junquera

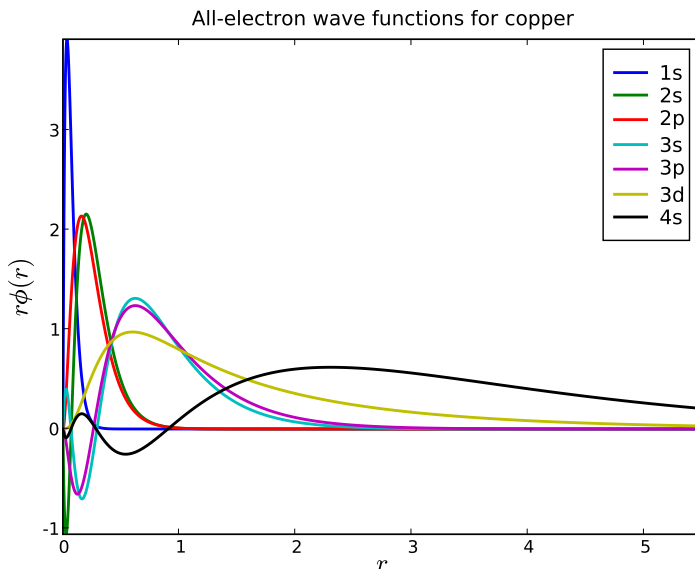


**Figure 5.1:** The all-electron Kohn-Sham wave functions for copper.

et al.[12]:

$$V_{\text{conf}}(r) = \begin{cases} 0 & r \leq r_{\text{conf}} \\ \frac{A}{r_{\text{conf}} - r} \exp\left(-\frac{r_{\text{conf}} - r_i}{r - r_i}\right) & r_i < r < r_{\text{conf}} \\ \infty & r_{\text{conf}} \leq r \end{cases} \quad (5.7)$$

The Kohn-Sham equations are solved exactly as in (5.4), except for the addition of the external potential  $V_{\text{conf}}$  to the effective potential, and the fact that we (still) integrate inwards from  $r_{\text{conf}}$  rather than infinity. As we shall see for most elements, good values of  $r_{\text{conf}}$  turn out to be around 5 to 8 Bohr with somewhat different values for each valence state. A smoothly confined wave function and the corresponding confinement potential are shown on Figure 5.2.

### 5.2.2 Pseudo orbital calculation

Knowing by now the *all-electron* Kohn-Sham wave functions  $|X_\mu\rangle$ , the next step is to derive the *pseudo* wave functions  $|\Phi_\mu\rangle$ , which means that we have to solve

$$|X_\mu\rangle = \hat{T}|\Phi_\mu\rangle = |\Phi_\mu\rangle + \sum_i \left( |\phi_i\rangle - |\tilde{\phi}_i\rangle \right) \langle \tilde{p}_i | \Phi_\mu \rangle \quad (5.8)$$

for  $|\Phi_\mu\rangle$ . Applying the  $i$ 'th projector  $\langle \tilde{p}_i |$  and using the orthogonality condition  $\langle \tilde{p}_i | \tilde{\phi}_j \rangle = \delta_{ij}$ , we obtain

$$\begin{aligned} \langle \tilde{p}_i | X_\mu \rangle &= \langle \tilde{p}_i | \Phi_\mu \rangle + \sum_j \langle \tilde{p}_i | \left( |\phi_j\rangle - |\tilde{\phi}_j\rangle \right) \langle \tilde{p}_j | \Phi_\mu \rangle \\ &= \sum_j \langle \tilde{p}_i | \phi_j \rangle \langle \tilde{p}_j | \Phi_\mu \rangle, \end{aligned} \quad (5.9)$$

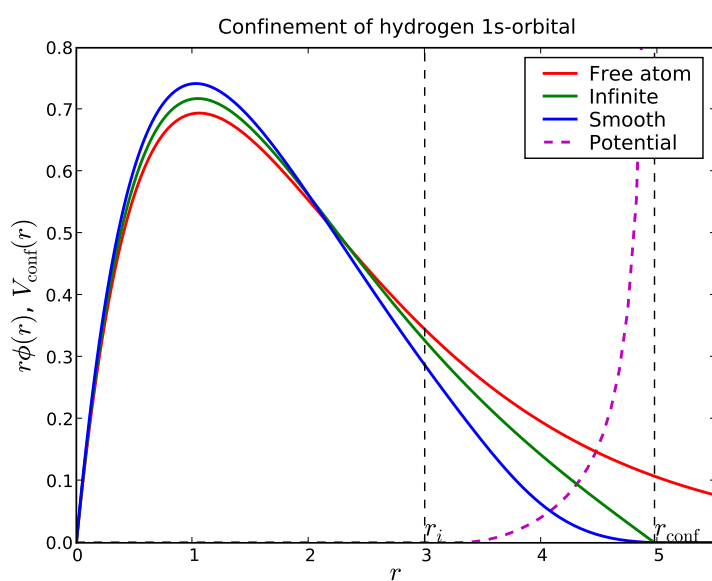


**Figure 5.2:** *The atomic orbital confinement scheme. The red curve corresponds to the unbounded wave function, while the green curve shows the wave function confined in a discontinuous infinite potential well. The blue curve is the smoothly confined wave function obtained by using the dashed potential.*

which is an ordinary system of linear equations for the inner products  $\langle \tilde{p}_j | \Phi_\mu \rangle$  which we can solve right away since the remaining entities are known. Knowing these inner products, it is a simple matter to write down the pseudo wave function by rearranging Equation (5.8):

$$|\Phi_\mu\rangle = |X_\mu\rangle + \sum_i \left( |\tilde{\phi}_i\rangle - |\phi_i\rangle \right) \langle \tilde{p}_i | \Phi_\mu \rangle. \quad (5.10)$$

Now, *if* the all-electron partial-wave expansion of  $|X_\mu\rangle$  were exact, this would be quite fine. However, the incompleteness of the partial waves and projectors causes the part of  $|X_\mu\rangle$  which cannot be represented as a linear combination of all-electron partial waves to spill out into  $|\Phi_\mu\rangle$ , resulting in oscillatory behaviour near  $r = 0$ . This effect can be seen in Figure 5.3 for a sodium wave function calculated using the *full expansion* (5.10). While this error tends to be small for most elements, it will still cause some degree of undesirable numerical behaviour.

To avoid this, we could alternatively make use of the “ideal” partial-wave expansion within the augmentation region

$$|\Phi_\mu\rangle = \sum_i |\tilde{\phi}_i\rangle \langle \tilde{p}_i | \Phi_\mu \rangle, \quad (5.11)$$

which assumes completeness of the projectors and pseudo partial waves. This expression has the obvious virtue of guaranteeing that the wave function behaves like a *pseudo* wave function near  $r = 0$ , but due to incompleteness outside the augmentation region, it will not become exactly 0 at the desired cutoff (the *pseudo-only* expansion in Figure 5.3). A reasonable solution, then, is to combine (5.10) and (5.11) by weighting the all-electron terms with a function  $w$  which approaches zero smoothly for  $r \rightarrow 0$ , but is equal to 1 outside the augmentation region. With this weighting function, we have

$$\Phi_\mu(\mathbf{r}) = \sum_i \langle \tilde{p}_i | \Phi_\mu \rangle \tilde{\phi}_i(\mathbf{r}) + w(r) \left( X_\mu(\mathbf{r}) - \sum_i \langle \tilde{p}_i | \Phi_\mu \rangle \phi_i(\mathbf{r}) \right). \quad (5.12)$$

This is the final expression for the first-zeta basis functions. The choice of  $w(r)$  is largely inconsequential as long as it is smooth at 0, since the all-electron and pseudo partial waves join each other smoothly already. Presently,

$$w(r) = \begin{cases} r^2/r_c^2, & r < r_c \\ 1, & r \geq r_c \end{cases}, \quad (5.13)$$

where  $r_c$  is the radius of the augmentation region.<sup>5</sup> This is the *weighted expansion* curve in Figure 5.3.

Finally, Figure 5.4 illustrates the full generation process: the calculated Kohn-Sham all-electron wave function (green) is localized within a certain radius (red, dashed), then transformed to a pseudo wave function (blue), differing from the all-electron one within the augmentation sphere of radius  $r_{\text{cut}}$ .

<sup>5</sup>One could also choose a function which approaches 1 smoothly, but when the cutoff is located exactly at  $r_c$ , this is unnecessary since the pseudo and all-electron partial waves join each other exactly here. This would only be a problem if  $w$  approached 1 *before* reaching  $r_c$ .

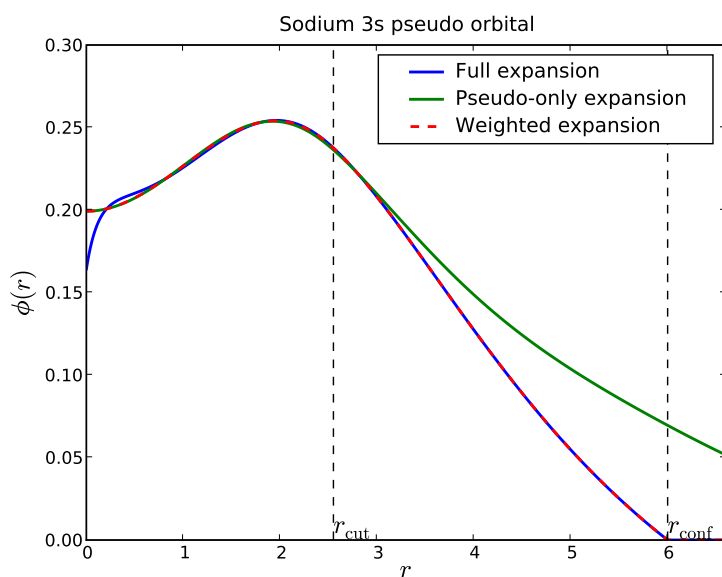


**Figure 5.3:** Pseudo basis function for the sodium 3s orbital calculated using the full expansion expression (5.10), the pseudo-partial wave expansion (5.11) and the weighted expansion (5.12), the latter being well-behaved both near and far from the atom. Note that the wave functions are not pre-multiplied by  $r$ .

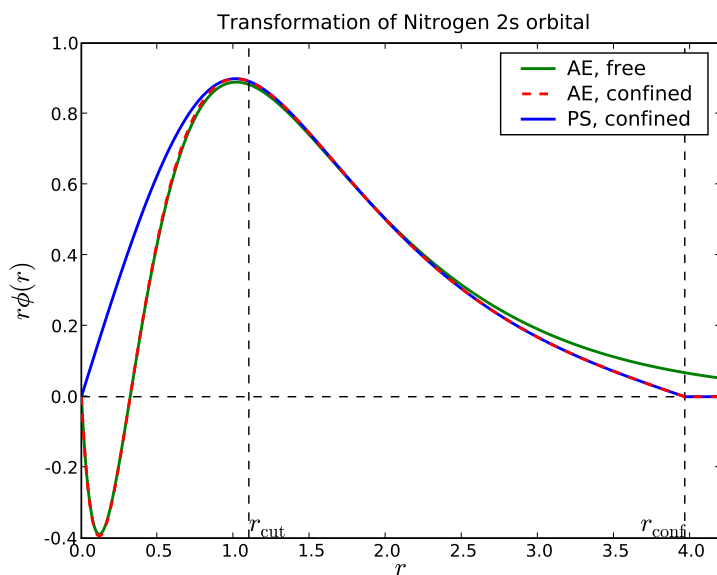


**Figure 5.4:** Summary of first-zeta basis function generation. The all-electron solution is localized using a confining potential, then transformed to a pseudo wave function.

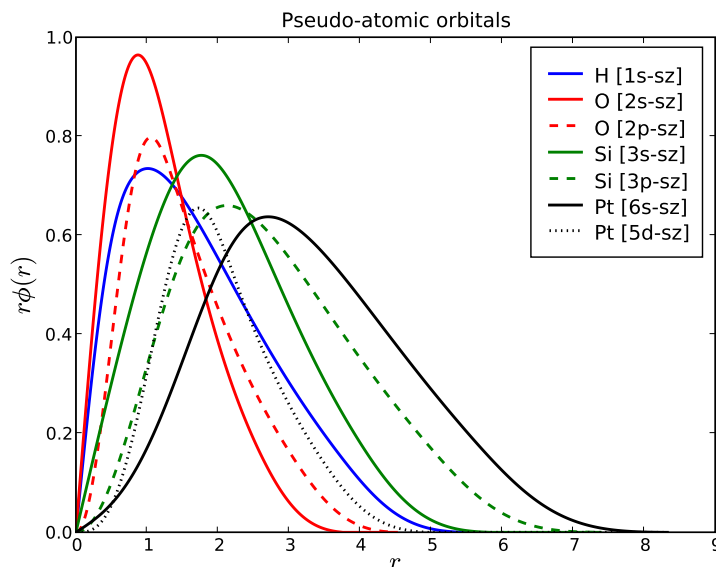


**Figure 5.5:** Miscellaneous PAOs for the fixed energy shift 0.3 eV. Lines are coloured by atomic species and styled depending on angular momentum.

### 5.2.3 Confinement radius selection by energy shift

Since some elements possess naturally larger orbitals than others, it is not elegant to have to specify each cutoff by hand to get reasonably proportioned localized wave functions. We employ once again the same approach as SIESTA to overcome this.[12] By specifying the wanted *energy shift*  $\Delta E$  of the confined orbital compared to the free-atom orbital, the corresponding confinement radius is uniquely determined in a uniform way for all elements.

Since we cannot straightforwardly calculate the cutoff for a particular energy, the method is implemented by means of bisection, repeating the following procedure until the energy shift is equal to the desired value within a certain threshold.

The energy shift is calculated for the two trial confinement radii  $r_{\text{small}}$  and  $r_{\text{large}}$ , which are selected such that the as of yet unknown, desired cutoff radius lies somewhere between them. The energy shift is then calculated at  $r_{\text{middle}}$  halfway between  $r_{\text{small}}$  and  $r_{\text{large}}$ , and depending on whether this energy here is larger or smaller than the desired one, either  $r_{\text{small}}$  or  $r_{\text{large}}$  is moved to  $r_{\text{middle}}$ , thus trapping the desired cutoff in a smaller interval. This process is repeated as required to meet some set tolerance.

With energy shifts between 0.1 and 0.3 eV, cutoff radii can be expected to lie between 3.5 Bohr (2s-orbitals of fluorine, oxygen) and 11.5 Bohr (Sodium 3s, lithium 2s), with most elements between 5 and 8 Bohr. Figure 5.5 shows a number of examples.

### 5.3 Multiple-zeta basis sets

Apart from the atomic orbitals themselves, there are no natural ways in which to further expand the basis sets. Several approaches have been formulated, and we have implemented two: the SIESTA method, which is inspired by the *split-valence* approach, and a second approach wherein the second-zeta basis function is obtained by differentiating the first-zeta one with respect to the orbital energy.

The split-valence approach originates from the use of basis functions which are linear combinations of Gaussians. To add extra radial functions for valence states, one or more of the most extended Gaussians of the orbital would be “freed” (or “split off”), becoming separate radial functions.[11]

In our case, the second radial function is obtained by subtracting a simple, rather arbitrary function  $\Delta\varphi(r)$  (which takes the role of the most extended Gaussian mentioned above) from the pseudo-atomic orbital. Thus we define

$$\varphi_{dz}(r) = \varphi_{sz}(r) - \Delta\varphi(r). \quad (5.14)$$

The function  $\Delta\varphi$  is defined as a polynomial within a certain radius  $r_{\text{split}}$ , and is equal to the first-zeta wave function outside, such that  $\varphi_{dz}$  becomes zero outside  $r_{\text{split}}$ :

$$\Delta\varphi(r) = \begin{cases} r^l(a - br^2) & r < r_{\text{split}} \\ \varphi_{sz}(r) & r \geq r_{\text{split}} \end{cases}. \quad (5.15)$$

The coefficients  $a$  and  $b$  are determined by requiring the polynomial to join the first-zeta wave function continuously and differentiably at  $r_{\text{split}}$ :

$$a - br_{\text{split}}^2 = \frac{\varphi_{sz}(r_{\text{split}})}{r_{\text{split}}^l} \quad (5.16)$$

$$-2br_{\text{split}} = \left[ \frac{d}{dr} \frac{\varphi_{sz}(r)}{r^l} \right]_{r=r_{\text{split}}}, \quad (5.17)$$

such that

$$b = -\frac{1}{r_{\text{split}}} \left[ \frac{d}{dr} \frac{\varphi_{sz}(r)}{r^l} \right]_{r=r_{\text{split}}}, \quad (5.18)$$

$$a = \frac{\varphi_{sz}(r_{\text{split}})}{r_{\text{split}}^l} + br_{\text{split}}^2. \quad (5.19)$$

With this approach, the second-zeta basis function will be confined within a smaller region than the first-zeta one. Figure 5.6 shows the first-zeta function, the subtracted function and resulting second-zeta function.

Once again, specifying the split radii for all the elements by hand would be a cumbersome endeavour. SIESTA already handles this in an elegant way, which we have likewise borrowed[12]: the split radius is determined by requiring the part of the first-zeta function outside  $r_{\text{split}}$  to have a particular norm  $T$ . On Figure 5.6, this area corresponds to the region below the graph between the two dashed lines.

The split radius is thus determined by

$$\int_{r_{\text{split}}}^{\infty} \varphi_{sz}^2(r) r^2 dr = T^2. \quad (5.20)$$

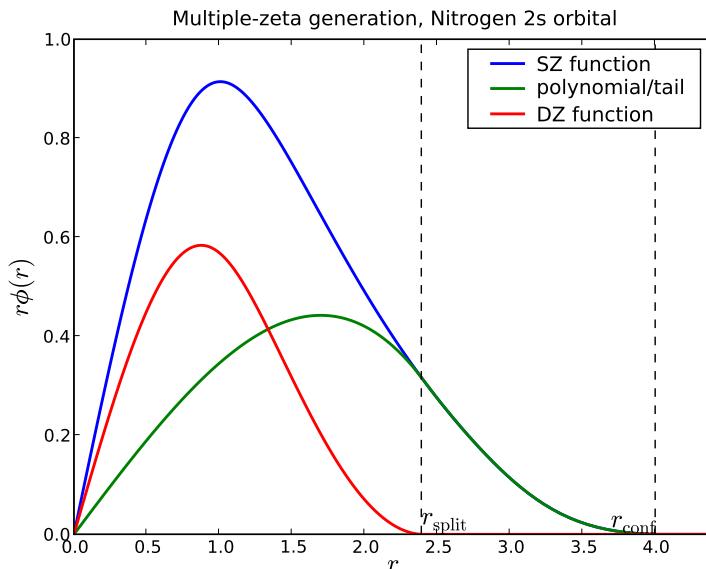


**Figure 5.6:** Generation of extra radial functions. The split radius is most practically determined by specifying the norm of the single-zeta tail beyond it.

The integration is performed by adding appropriately weighted, squared function values, starting at infinity (or rather the right-most grid point) and moving inwards until the accumulated sum totals  $T^2$ . This prevents the special normalization issues that pertain to the pseudo-character of the wave function near  $r = 0$  from affecting the result.

We have found that using a value of around  $T^2 = 0.03$ , or  $T \approx 0.17$ , tends to produce the lowest total energies. This is essentially equal to the value  $T \approx 0.15$  reported for SIESTA.[11]

### 5.3.1 Energy derivative approach

A different way to generate an extra orbital is to take the derivative of the pseudo-atomic orbital with respect to the orbital energy. This scheme is used among other things in linear augmented plane-wave methods.[19, pp. 345-348]

The second-zeta function is here defined as

$$\varphi_{dz}(r) = \frac{d\varphi_{sz}(r)}{d\Delta E}, \quad (5.21)$$

which can be implemented by calculating  $\varphi_{sz}(r)$  for two slightly different energy shifts (actually using two adjacent or otherwise close confinement radii) and subtracting. Each function is normalized before subtraction. This is the usual way to do it, because it guarantees that  $\varphi_{dz}$  becomes orthogonal to  $\varphi_{sz}$ , although this property is not in fact useful to us. Since we are using *pseudo* orbitals for  $\varphi_{sz}$ , we should note that it does not in fact matter whether the derivative is taken *before* or *after* the transformation to pseudo wave functions.



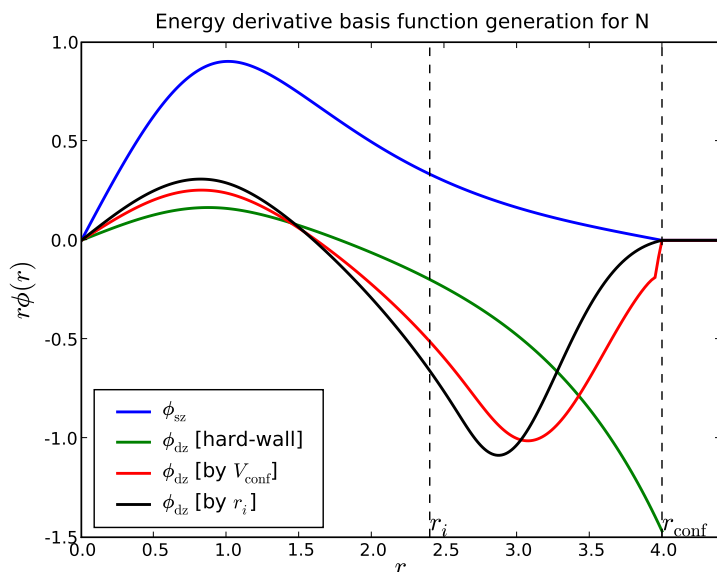


**Figure 5.7:** *The energy derivative approach. Shows a first-zeta orbital and second-zeta orbitals corresponding to the infinite hard-wall potential method, a smooth confinement potential and finally an approach where the derivative is taken with respect to the inner cutoff parameter  $r_i$  of the potential.*

When  $\varphi_{sz}$  is calculated using the infinite hard-wall potential, the resulting basis function will be discontinuous and thus useless. By using a smooth confinement potential, the function becomes almost continuous but still has a small discontinuity at the cutoff. Finally, if *instead* of differentiating by  $\Delta E$ , we differentiate by the inner cutoff parameter  $r_i$  of the confinement potential (5.7), the function becomes smooth. These different methods are shown in Figure 5.7. Using lower values of  $r_i$  to define the potential, the features of the derivative function can be shifted towards smaller  $r$ .

Generally the basis functions generated by this method are less smooth than those of the previous section, with the further drawback that they have somewhat larger curvature far from the nucleus (while this effect appears disproportionately large on Figure 5.7 due to the  $r\phi(r)$  axis, it is in fact a relatively modest problem). So far, we observe that calculated energies are consistently higher for DZ basis sets when using this scheme compared to the split-valence-like scheme of the previous section. For this reason we consider the previous approach better, although it may well be possible to obtain more suitable shapes using different confinement potentials.

## 5.4 Polarization functions

We have now seen considered ways to construct basis functions that correspond to the valence states on an atom. Polarization functions, as mentioned, are basis

functions corresponding to angular momenta not present among the valence states, which will probably be needed to properly describe the wave functions in a bonding environment.

### 5.4.1 Methods for selecting polarization functions

We have considered several methods:

- The obvious possibility is to use the unoccupied atomic orbitals with appropriate angular momentum. This has the drawback that the orbitals in question are generally more delocalized than the valence states, and possibly unbound. Although they can be confined using the same method as for the first-zeta functions, we find this method somewhat unphysical, since the choice of confinement potential will largely determine the shape.
- SIESTA polarizes one of the valence orbitals directly by applying a small electric field, then using perturbation theory to derive a differential equation for the polarization function[11].
- Another possibility is to construct a reference system such as a molecule or a crystal, and obtain a polarization function by interpolating the actual wave functions calculated on the grid. This will be done below.
- Finally one can just choose a function of some simple form. It turns out that this simple method is sufficient since the functional form can be chosen in such a way as to universally resemble the results found by the interpolation method.

The next section details the reference wave function interpolation scheme.

### 5.4.2 Wave function interpolation using Gaussians

Suppose we want to find a polarization function for a particular atom corresponding to a particular angular momentum quantum number  $l$ . The plan is to construct a *reference* system, such as a molecule, for which we calculate the wave functions using the grid code.

Then we will choose a number of primitive functions, and construct the polarization function from the linear combination of these which best reproduces the  $l$ -character component of the reference wave function around the atom under consideration.

Note that we want, like before, *one* radial function  $\varphi(r)$  shared by  $2l + 1$  basis functions with different spherical harmonic angular parts  $Y_{lm}$ , such that

$$\Phi_m(\mathbf{r}) = \varphi(r)Y_{lm}(\hat{\mathbf{r}}) \quad \text{for all } m = -l \dots l, \quad (5.22)$$

where the radial function is composed of primitive Gaussian-like, localized functions  $\chi_i$ , which we shall call *quasi-Gaussians*:

$$\varphi(r) = \sum_i c_i \chi_i(r), \quad \chi_i(r) = \begin{cases} r^l e^{-\alpha_i r^2} - r^l (a_i - b_i r^2), & r < r_{\text{conf}} \\ 0 & r \geq r_{\text{conf}} \end{cases}, \quad (5.23)$$

where  $a_i$  and  $b_i$  are chosen to make  $\chi_i$  smooth at  $r_{\text{conf}}$ :

$$a_i = (1 + \alpha_i r_{\text{conf}}^2) e^{-\alpha_i r_{\text{conf}}^2}, \quad (5.24)$$

$$b_i = \alpha_i e^{-\alpha_i r_{\text{conf}}^2}. \quad (5.25)$$

For future convenience, let

$$X_{im}(\mathbf{r}) = \chi_i(r) Y_{lm}(\hat{\mathbf{r}}) \quad (5.26)$$

denote the primitive functions including angular dependence. The Gaussian-like functions are *not* chosen because of the convenient properties of Gaussians (products of Gaussians being Gaussians, exact integration and so on, which would not work anyway due to the polynomial correction), but simply because they resemble pseudo wave functions.

Choosing a set of  $\alpha_i$  then defines a basis of primitive functions. The next step is to determine the expansion coefficients  $c_i$  by maximizing the overlap with the pre-calculated wave functions of some reference system (usually being the dimer corresponding to the atom whose polarization function we wish to calculate, but this could also be a periodic system with multiple  $k$ -points). To do this, we define a projection operator

$$\hat{P}^{\mathbf{k}} = \sum_n |\bar{\psi}_n^{\mathbf{k}}\rangle \langle \bar{\psi}_n^{\mathbf{k}}|, \quad (5.27)$$

where  $|\bar{\psi}_n^{\mathbf{k}}\rangle$  are orthonormalized pseudo wave functions, such that  $\langle \bar{\psi}_n^{\mathbf{k}} | \bar{\psi}_{n'}^{\mathbf{k}'} \rangle = \delta_{\mathbf{k}\mathbf{k}'} \delta_{nn'}$ . The wave functions are inherently Bloch orthogonal, but band orthogonality must be enforced – this is achieved by performing Gram-Schmidt orthogonalization. The plan is then to calculate the coefficients that maximize the overlap expression

$$B = \sum_{\mathbf{k}m} \frac{||\hat{P}^{\mathbf{k}} \Phi_m^{\mathbf{k}}||^2}{||\Phi_m^{\mathbf{k}}||^2}, \quad (5.28)$$

where the  $k$ -point specific polarization function  $\Phi_m^{\mathbf{k}}$  is obtained from the canonical one in (5.22) by summation over neighbouring cell coordinates  $\mathbf{R}_c$  with appropriate phases. Hence

$$\Phi_m^{\mathbf{k}}(\mathbf{r}) = \sum_{\mathbf{R}_c} e^{i\mathbf{k}\cdot\mathbf{R}_c} \Phi_m(\mathbf{r} - \mathbf{R}_c) = \sum_{i\mathbf{R}_c} c_i e^{i\mathbf{k}\cdot\mathbf{R}_c} X_{im}^{\mathbf{R}_c}(\mathbf{r}) \quad (5.29)$$

where we have defined  $X_{im}^{\mathbf{R}_c}$  to mean the displacement of  $X_{im}$  by  $\mathbf{R}_c$ . The overlap measure  $B$  must of course be rewritten to depend explicitly on the coefficients. First,

$$\begin{aligned} ||\hat{P}^{\mathbf{k}} \Phi_m^{\mathbf{k}}||^2 &= \sum_n \langle \Phi_m^{\mathbf{k}} | \bar{\psi}_n^{\mathbf{k}} \rangle \langle \bar{\psi}_n^{\mathbf{k}} | \Phi_m^{\mathbf{k}} \rangle \\ &= \sum_{nij} \sum_{\mathbf{R}_c \mathbf{R}'_c} e^{i\mathbf{k}\cdot(\mathbf{R}'_c - \mathbf{R}_c)} c_i^* \langle X_{im}^{\mathbf{R}_c} | \bar{\psi}_n^{\mathbf{k}} \rangle \langle \bar{\psi}_n^{\mathbf{k}} | X_{jm}^{\mathbf{R}'_c} \rangle c_j. \end{aligned} \quad (5.30)$$

Likewise,

$$||\Phi_m^{\mathbf{k}}||^2 = \sum_{ij} \sum_{\mathbf{R}_c \mathbf{R}'_c} e^{i\mathbf{k}\cdot(\mathbf{R}'_c - \mathbf{R}_c)} c_i^* \langle X_{im}^{\mathbf{R}_c} | X_{jm}^{\mathbf{R}'_c} \rangle c_j. \quad (5.31)$$

The overlap measure  $B$  can then be expressed in terms of matrices,

$$B = \sum_{\mathbf{k}m} \frac{\mathbf{c}^\dagger \mathbf{S}_m^{\mathbf{k}} \mathbf{c}}{\mathbf{c}^\dagger \boldsymbol{\sigma}_m^{\mathbf{k}} \mathbf{c}}, \quad (5.32)$$

where  $\mathbf{c}$  is the column matrix of coefficients  $c_i$ , and the matrix elements are

$$S_{mij}^{\mathbf{k}} = \sum_{n\mathbf{R}_c\mathbf{R}'_c} e^{i\mathbf{k}\cdot(\mathbf{R}_c-\mathbf{R}'_c)} \langle X_{im}^{\mathbf{R}_c} | \bar{\psi}_n \rangle \langle \bar{\psi}_n | X_{jm}^{\mathbf{R}'_c} \rangle, \quad (5.33)$$

$$\sigma_{mij}^{\mathbf{k}} = \sum_{\mathbf{R}_c\mathbf{R}'_c} e^{i\mathbf{k}\cdot(\mathbf{R}_c-\mathbf{R}'_c)} \langle X_{im}^{\mathbf{R}_c} | X_{jm}^{\mathbf{R}'_c} \rangle. \quad (5.34)$$

While it might be possible to simplify the optimization problem by setting the derivative of  $B$  with respect to the coefficients to zero, so far we have written an implementation of the Nelder-Mead or *downhill simplex* algorithm[18, pp. 305–309] to maximize the overlap, selecting an initial *simplex* in the space of coefficients, then running the algorithm until a certain threshold is reached. All pertinent inner products can be pre-evaluated. This operation is equivalent to the cross-grid type product integrations  $\langle \bar{p}_i^a | \bar{\psi}_n^{\mathbf{k}} \rangle$  from Chapter 3 for Bloch wave functions. Even  $s_{mij}$  are calculated in this way by putting one of them on the grid, since this will ensure that the matrix elements are subject to the same numerical issues.

The algorithm converges consistently for any tested number of primitives (between one and thirty). The coefficients will, since there is no norm-enforcing mechanism, tend to diverge: if many primitives are used, some coefficients can be thousands of times larger than others, effectively disregarding part of the primitive basis. This does not appear to be harmful – the generated polarization function is consistent regardless of the number of Gaussians, see Figure 5.8.

### 5.4.3 Generated functions

Rather than specifying the Gaussian decay parameters  $\alpha_i$ , it is practical to specify *characteristic lengths*  $r_{\text{ch},i} = 1/\sqrt{\alpha_i}$ . In the following plots, characteristic lengths are equidistantly distributed between 1 Bohr and half the polarization function cutoff.

Figure 5.9 shows examples of generated polarization functions. The cutoff is in each of these cases equal to the largest cutoff found among the single-zeta basis functions with default parameters. Some of the functions (nitrogen, oxygen and fluorine) appear “hunchbacked” to varying extent.

This hunchback effect probably appears because the polarization function “wants” to describe parts of the reference wave functions around other atoms, thus resulting in a more delocalized distribution which would not appear if the projection scheme took into account that those atoms were equipped with basis functions of their own (this, of course, is a rather *silly* error which can be fixed by using a better projection scheme). This prompts the optimizer to select a very large coefficient to the most extended primitive, whereas the second-most extended primitive gets a proportionately large, negative coefficient to cancel out this effect for smaller  $r$  (with more primitives and sharper confinement, this numerical instability can in fact result in several such oscillations).<sup>6</sup>

<sup>6</sup>An interesting test is to construct an analytic, fictional reference wave function with the

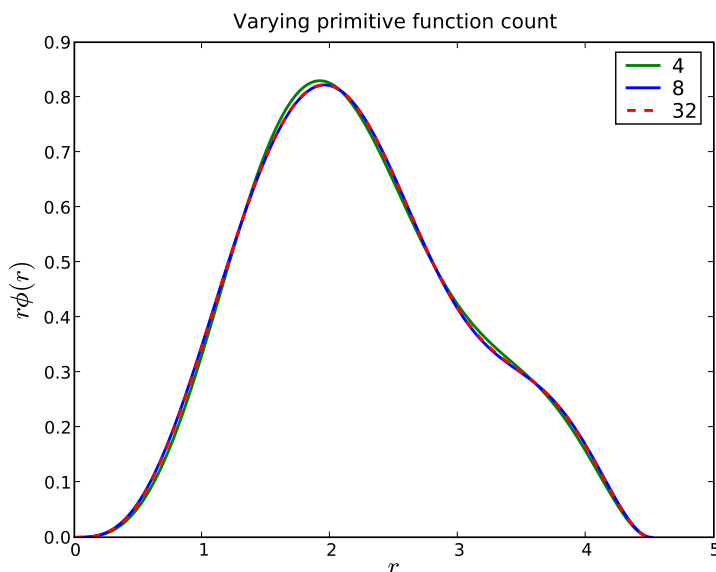


**Figure 5.8:** Polarization functions for oxygen in  $H_2O$  with varying numbers of primitive functions with evenly distributed characteristic radii.

The hunchback effect is quite dependent on which reference system is used. For some reference systems, such as  $Cl_2$  and  $Be_2$ , disproportionately large cutoff radii (e.g. more than 1.5 times the largest first-zeta cutoff) are required for the polarization function to behave smoothly.

The hunchback effect is particularly pronounced in periodic systems with more than one atom in the unit cell, which is quite unsurprising considering that the electron cloud is delocalized. In the case of a *single*-atom cell, however, the projection scheme performs better, and produces reasonably well-behaved functions. This, of course, requires using simple, cubic crystals which is not physically accurate in general.

As mentioned, a different projection scheme would be capable of taking care of this problem, such as the one described by Gusso[14]. As it will turn out in the next section, however, the exact shape of the polarization function is not all that important.

#### 5.4.4 Single-Gaussian polarization functions

On closer inspection, it is evident that many of the generated polarization functions have quite similar overall shapes, though individual cutoffs vary significantly.

Figure 5.10 shows several interpolated polarization functions plotted with scaled  $r$ -axis (for most elements the scale corresponds to the cutoff, but this

---

shape of a quasi-Gaussian, and observe that this is interpolated correctly. Reducing the cutoffs of the interpolating functions below the cutoff of the reference function will then result in the hunchback effect, and further reduction can result in quite violent oscillations.

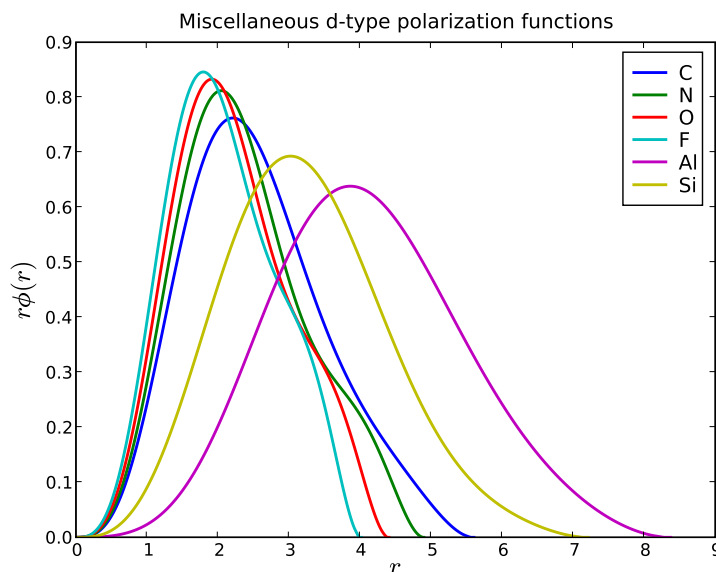


**Figure 5.9:** Miscellaneous polarization functions, some of which are “hunchbacked”. Calculated using reference molecules  $\text{CH}_4$ ,  $\text{NH}_3$ ,  $\text{H}_2\text{O}$ ,  $\text{HF}$ ,  $\text{AlCl}_3$  and  $\text{SiO}$ . Each function is composed of four primitive Gaussian-like orbitals.

is not true for all of them). As can be seen, particularly for low values of  $r$ , the functions exhibit a very similar behaviour.<sup>7</sup> The part of the wave function located far from the atom is likely to be considerably influenced by the bonding environment, which means its exact shape here might be less important.

Therefore, this near-universal behaviour can be well described by a single, appropriately chosen Gaussian. The Gaussian shown on 5.10 has a characteristic radius of 0.35 (measured on the  $r/r_0$  axis, not in Bohr radii).

With this in mind, the present polarization function selection method is to use a single quasi-Gaussian with a characteristic length of 0.25 times the cutoff of the largest pseudo-atomic orbital calculated with a confinement energy of 0.3 eV. This is just a temporary solution until more test results are available, so a more generic selection method can be implemented.

## 5.5 Basis set parameters in practice

By this point, we have the following parameters to consider when creating basis sets:

- The energy shift  $\Delta E$  defining the first-zeta cutoff  $r_{\text{conf}}$ . Sensible values[12] are  $0.1\text{eV} \leq E_C \leq 0.3\text{eV}$ , although we find that lower values can be neces-

<sup>7</sup>The suspicious reader might suggest that this is because each function has just one dominant Gaussian near  $r = 0$ . This, however is not true. The least extended Gaussians can be chosen differently, but the behaviour of the interpolated function remains largely unaffected.

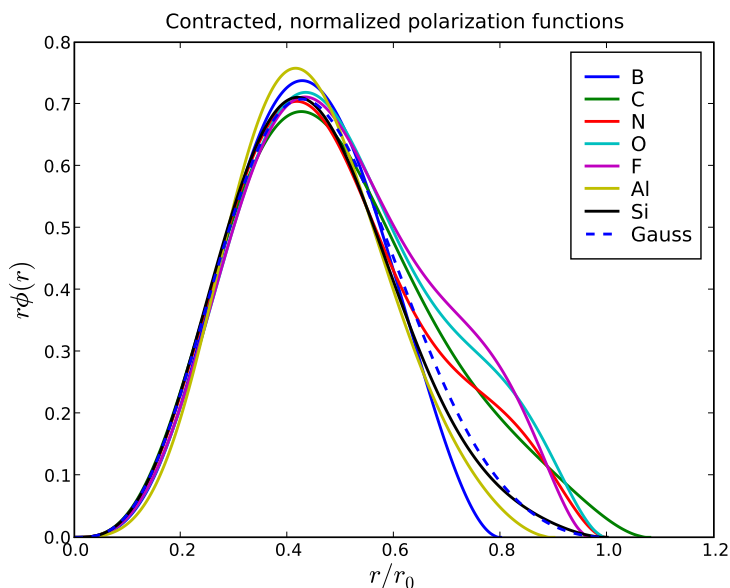


**Figure 5.10:** Contracted and normalized  $d$ -type 4-Gaussian polarization functions for various elements. The overall shape appears to be universal for small  $r$ . The dashed line is a hand-fitted quasi-Gaussian.

sary, particularly when concerned with energy calculations on molecules.

- The confinement potential parameters  $A$  and  $r_i$  in (5.7), if using the smooth confinement scheme. The default values are  $A = 12$  and  $r_i = 0.6r_{\text{conf}}$ .
- The tail norm values that define the split radii  $r_{\text{split}}$  for each multiple-zeta basis function. The default is a squared tail norm of  $T^2 = 0.03$  for the second zeta function. Good values for subsequent zeta-functions are not yet known, but the default value is  $T^2 = 0.1$  for the following one.
- The characteristic radius  $r_{\text{ch}}$  which defines the shape of the polarization function, along with the polarization function cutoff. The cutoff is generally chosen equal to the largest present single-zeta cutoff, and we have found so far that for hydrogen through chlorine,  $r_{\text{ch}} = .25r_{\text{conf}}^{\text{sz}}$  generally produce low energies for  $\Delta E = 0.3$  eV. The wave function interpolation scheme can still be necessary to estimate good values of  $r_{\text{ch}}$  for transition metals and generally elements with high atomic numbers. When adding more than one polarization function, the present behaviour is to use the usual multiple-zeta scheme rather than adding more Gaussians.

Generating a basis set generally takes a few seconds to around one minute. Most CPU time is spent solving the all-electron Kohn-Sham problem, although using periodic reference systems for the polarization function can be quite time-consuming if the cutoff spans many cells.

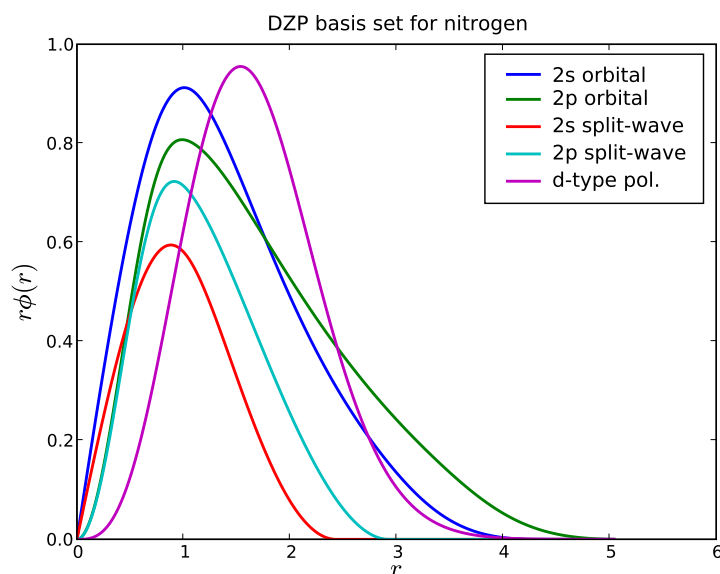


**Figure 5.11:** Double-zeta polarized basis set for oxygen. This is the canonical type of basis set presently used for serious calculations, generated with default parameters.

Figure 5.11 shows the default basis set for oxygen. This is a double-zeta polarized basis set, using the tail-norm method for the second-zeta functions and a single quasi-Gaussian for polarization. With a total of five radial functions, remember that the true number of basis functions during a calculation is larger due to the multiple angular parts. This atom possesses thirteen basis functions: one for each s-type, three for each p-type and five for the d-type polarization function.

### 5.5.1 Notes on state selection

For the elements hydrogen through calcium, the valence states are either s-states only or both s- and p-states. These elements are therefore assigned d-type polarization functions. Transition metals, on the contrary, having s- and d-type valence states, get polarization functions of type p. Polarization functions with larger angular momentum have not been tested systematically yet.

In the rare case that an element has no occupied valence s-orbital, it is very important to add an s-type orbital, which should not just be considered a polarization function. As it turns out, the *only* element with this behaviour is palladium, unless using non-standard definitions of valence versus core states.

Having now described the methods used to generate basis functions, next chapter compares various basis sets with grid-based calculations.



# Chapter 6

## Basis set test results

This chapter presents the results of different tests using the localized basis functions, comparing results to similar grid-based calculations. We will first present some test results performed on simple molecules and atoms, then consider adsorption energies in more complex systems.

We note first that it is not very useful to compare *total* energies calculated using grid-based versus atomic basis set methods. The grid-based total energy is generally much lower but does not say much about the actual accuracy that can be obtained with basis sets, since the accuracy is determined to a large extent by the inherent error cancellation due to the subtraction in atomization energies.

### 6.1 Molecule tests

In this section we calculate the atomization energies of molecules, comparing different basis sets with each other and equivalent grid-based energies. The particular calculations presented in this section have been performed by Marco Vanin, using the basis set generation code of Chapter 5 [17].

The atomization energy  $\Delta E_a$  of a molecule is the difference in total energy between the molecule and its constituent atoms:

$$\Delta E_a = E_{\text{mol}} - \sum_{\text{atoms}} E_{\text{atom}} \quad (6.1)$$

We consider the G2-1 set of molecules with experimentally obtained geometries. These are available in the module `gpaw.testing.g2` included with GPAW. All calculations are done using cells of  $12 \times 13 \times 14$  Å and a grid spacing of  $h = 0.18$  Å. Calculations on systems with non-zero magnetic moments are of course performed as spin-polarized. This means isolated atoms are spin-polarized, while most, but not all, molecules are spin-paired.

Figure 6.1 shows the performance of DZ, DZP, TZP and TZDP basis sets. Figure 6.1a corresponds to a confinement energy shift of  $\Delta E = 0.1$  eV used when generating the first-zeta basis functions, whereas 6.1b uses an energy of  $\Delta E = 0.01$  eV. Remaining basis set parameters are defaults (see Section 5.5).

A few observations will help to understand the graphs. In terms of *total* energies, the addition of extra basis vectors will always *lower* the energy, conferring extra variational freedom to the wave function. Since the isolated atoms

are described by atomic orbitals, it would at first appear reasonable to assume that the corresponding energies are very close to exact. But this is not true for two reasons:

- The confinement energy shifts  $\Delta E$  add to the total energy for each valence state.
- The atomic calculation generating the basis functions is spin-paired.

The first of these effects is largely negated by using an energy shift of 0.01 eV as in Figure 6.1b, and the corresponding decrease of atomic energies explains why the calculated energies here generally lie *higher* (since the atomic energies are subtracted) than in 6.1a.

Results using the DZP basis or larger basis sets mostly lie within 0.5 eV of grid values. It is evident that the DZP basis is the smallest which yields reasonable results, and that the DZP results for most elements are only slightly improved by adding further basis functions. While using triple-zeta basis sets can improve the results for some systems, the addition of an extra polarization function only yields very marginal improvements.

## 6.2 Adsorption energies

To test basis set performance under more realistic conditions, we calculate adsorption energies for a collection of more complex systems, again comparing the results to grid-based calculations. Vivien Petzold has kindly provided a collection of relaxed geometries for such systems calculated in GPAW using grid-based wave functions. One such system is shown on Figure 6.2.

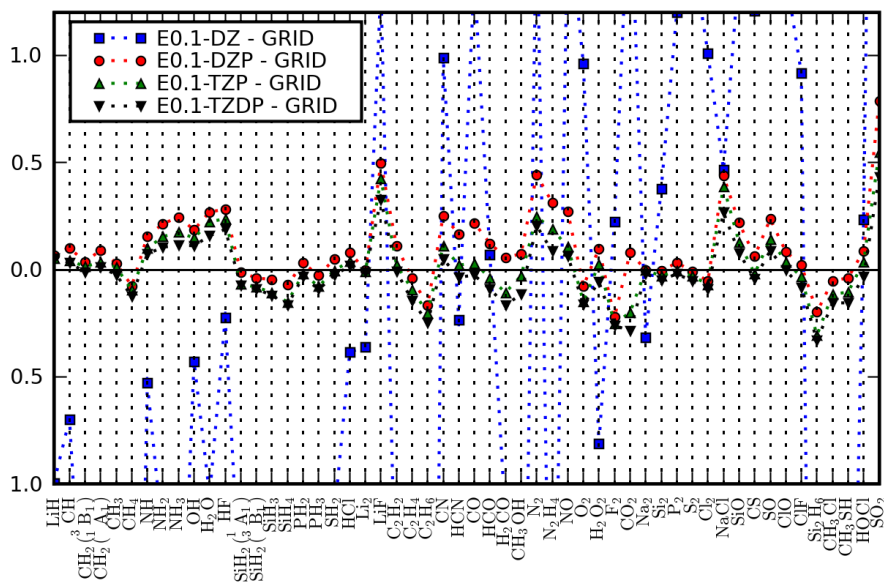
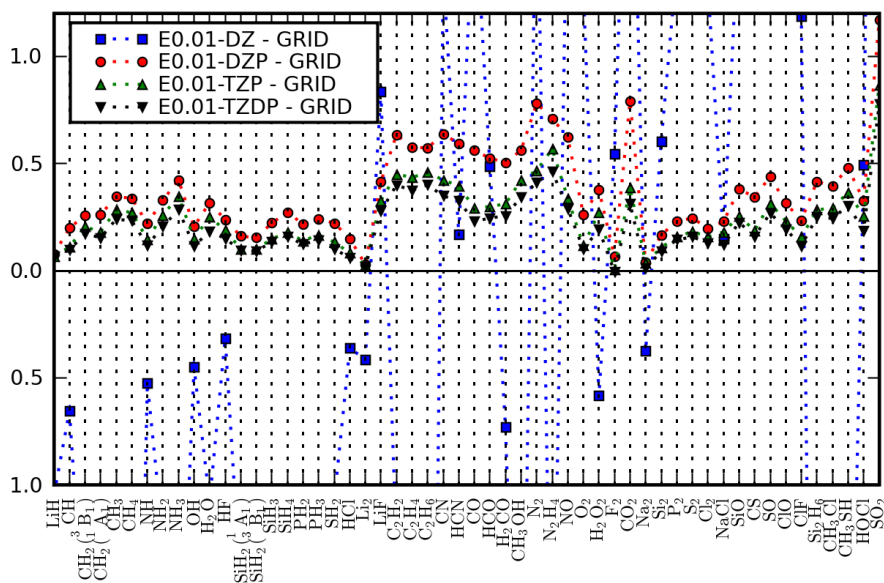
We consider the adsorption of O, NO and CO onto different surfaces of palladium and rhodium. To calculate an adsorption energy we must calculate the total energy  $E_{\text{mol}}$  of the isolated molecule (or atom), the energy  $E_{\text{surf}}$  of the empty crystal surface and the energy  $E_{\text{ads}}$  of the combined system, where the molecule has been adsorbed onto the surface. The adsorption energy is then given by the difference

$$\Delta E_{\text{ads}} = E_{\text{full}} - E_{\text{surf}} - E_{\text{mol}}. \quad (6.2)$$

The calculations are carried out with the same parameters used for the relaxation.<sup>1</sup> The molecules have DZP basis sets with an energy shift of  $\Delta E = 0.01$  eV, while the metals have  $\Delta E = 0.1$  eV. The calculations generally use  $8 \times 8 \times 1$  or  $8 \times 10 \times 1$   $k$ -points.

The results are shown in Table 6.1. *Note that all total energies and adsorption energies are in fact negative.* The ‘‘Site’’ column denotes the type of location on the surface where the molecule is adsorbed. Hollow sites are denoted by hol, bridge sites by brd. Fcc sites correspond to a location where an atom would be placed in an fcc crystal (as opposed to hcp). The last three columns compare the adsorption energies for basis-set and grid calculations.

<sup>1</sup>In order to make the calculation converge it is generally necessary to use a non-standard density mixer (see Section 2.4), which is more conservative in the sense that it uses a smaller than normal weight for newly calculated densities. It is common to weight the new density by only 0.1 when doing calculations on metals, while we find that it has to be reduced even further, to 0.06.

(a)  $\Delta E = 0.1eV$ (b)  $\Delta E = 0.01eV$ 

**Figure 6.1:** Atomization energies of the G2-1 dataset of small molecules for different basis sets and for two different energy shifts. Energies are relative to the grid values. The unit is eV. This figure is borrowed from Marco Vanin [17].

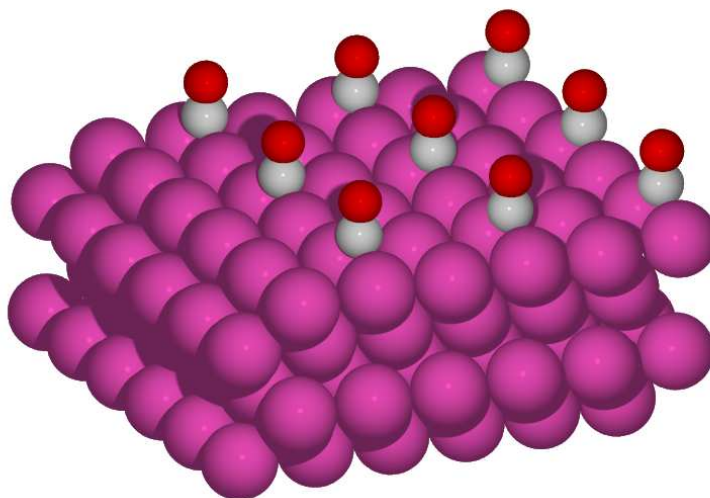


**Figure 6.2:** *CO adsorbed on a bridge site of a Pd (100) surface. This figure shows the basic cell repeated  $3 \times 3$  times.*

The calculated adsorption energies differ by between 0.1 eV and 1 eV, most errors being around 0.6 eV. The larger deviations may well be due to the *basis set superposition error*. To explain this, we consider two entities, such as a molecule and a crystal surface. When brought close together, each entity can “borrow” degrees of freedom which are less important to the other entity, thereby “enlarging” its own basis set. This results in lower energies of the composite system, which is consistent with our results.

The basis set superposition error can be remedied by making sure that the same basis is available in all systems. For example, in the case of the empty surface calculation, the adsorption site is equipped with “ghost orbitals” corresponding to the basis functions that *would* have been there if the molecule were present. It is also likely that the results could be improved by using a larger basis set – we have already seen that TZP basis sets can improve results appreciably for some systems.

### 6.3 Conclusion

We have tested the generated basis sets by calculating atomization energies and adsorption energies. In order to get reasonably converged atomization energies, it is necessary to use DZP basis sets or better. Using larger basis sets than DZP can bring about improvements for certain systems, but many systems are well described with DZP.

As for adsorption energies, we do not yet find the present implementation to yield results with desirable accuracy. A large part of the error may well be caused by the basis set superposition error, which can be eliminated in a systematic way.

Surf.	Ads.	Site	$E_{\text{surf}}^{\text{grid}}$	$E_{\text{surf}}^{\text{lcao}}$	$E_{\text{mol}}^{\text{grid}}$	$E_{\text{mol}}^{\text{lcao}}$	$E_{\text{full}}^{\text{grid}}$	$E_{\text{full}}^{\text{lcao}}$	$E_{\text{ads}}^{\text{grid}}$	$E_{\text{ads}}^{\text{lcao}}$	Err
Rh100	O	hol	106.31	91.42	2.18	1.79	113.53	98.75	5.04	5.53	0.50
Rh100	NO	brd	106.31	91.42	12.99	11.61	121.78	106.28	2.48	3.25	0.77
Rh100	CO	brd	106.31	91.42	15.23	14.14	123.54	108.45	2.00	2.90	0.89
Pd111	O	fcc	41.71	32.81	2.20	1.79	48.20	39.00	4.29	4.41	0.11
Pd111	NO	fcc	41.71	32.81	12.99	11.61	56.94	47.16	2.24	2.75	0.51
Pd111	CO	fcc	41.71	32.81	15.25	14.13	58.94	49.49	1.98	2.55	0.57
Pd100	O	hol	55.89	44.02	2.20	1.79	62.31	50.22	4.22	4.42	0.20
Pd100	NO	hol	55.89	44.02	12.99	11.61	70.93	58.28	2.05	2.65	0.61
Pd100	CO	brd	55.89	44.02	15.25	14.13	73.01	60.54	1.86	2.39	0.53

**Table 6.1:** Adsorption energies in eV calculated with grid and basis sets. The energies obtained using basis sets consistently predict more stable adsorbed states. All energies are negative. While absolute energies deviate considerably between the two methods, error cancellation yields much smaller final deviations.



## Chapter 7

# Force calculations in LCAO

The purpose of this chapter is to calculate the force  $\mathbf{F}^a$  on an atom  $a$  within the PAW formalism, thus allowing e.g. molecular dynamics simulations.

This force is equal to the derivative of the total energy  $E$  with respect to the nuclear coordinates  $\mathbf{R}^a$  of  $a$ . The force expression which applies to the grid-based case does not apply in our case because of the complication that the basis functions move along with the atoms.

### 7.1 Strategic considerations

The plan is to use the chain rule on  $\frac{\partial E}{\partial \mathbf{R}^a}$  after identifying a suitable set of intermediate parameters through which to differentiate. One could also differentiate the energy expression term by term, but using the chain rule is probably easier, since several useful partial derivatives (such as  $\tilde{v}_{\text{eff}}(\mathbf{r}) = \frac{\delta E}{\delta \tilde{n}}$ , etc.) appear more readily this way.

In the following, the symbol  $a$  shall refer to the particular atom whose forces are about to be calculated, while arbitrary atoms will be indexed by  $b$  to avoid notational confusion. Recall that the total energy (3.44) is

$$E = \tilde{E} + \sum_b (E^b - \tilde{E}^b), \quad (7.1)$$

where

$$\begin{aligned} \tilde{E} = & \sum_{\mu\nu} \rho_{\nu\mu} \langle \Phi_\mu | -\frac{1}{2} \nabla^2 | \Phi_\nu \rangle + \frac{1}{2} \int \frac{\tilde{\rho}(\mathbf{r}) \tilde{\rho}(\mathbf{r}')}{\|\mathbf{r} - \mathbf{r}'\|} d^3\mathbf{r} d^3\mathbf{r}' \\ & + \sum_b \int \tilde{n}(\mathbf{r}) \tilde{v}^b(\mathbf{r}) d^3\mathbf{r} + E_{\text{xc}}[\tilde{n}]. \end{aligned} \quad (7.2)$$

The atomic contributions  $E^b$  and  $\tilde{E}^b$ , which we do not bother listing here, can be lobbed together in an expression  $\Delta E^b = E^b - \tilde{E}^b$ . This is a function of the atomic density matrices  $D_{ij}^b$  and some atomic variables, i.e. the only dependence on environment, and thereby nuclear position, is through  $D_{ij}^b$ . Hence  $\Delta E^b$  is a function *only* of  $D_{ij}^b$  for the purposes of differentiation with respect to nuclear coordinates.

The pseudo charge density  $\tilde{\rho}$  which completely determines the Coulombic contribution to  $\tilde{E}$  is

$$\tilde{\rho}(\mathbf{r}) = \tilde{n}(\mathbf{r}) + \sum_{bL} Q_L^b \tilde{g}_L^b(\mathbf{r}), \quad (7.3)$$

where the expansion coefficients  $Q_L^b$  depend on  $D_{ij}^b$  plus some internal, atomic variables which are constant. For this reason,  $\tilde{\rho}$  depends on  $\tilde{n}$ ,  $D_{ij}^b$  and the location of the atom-centered functions  $\tilde{g}_L^b$ .

With this and (7.2) in mind, the total energy will be regarded as a function of precisely the following variables, where each variable is itself dependent on the nuclear coordinates in some manner yet to be described:

- The density matrix elements  $\rho_{\mu\nu}$ .
- The kinetic energy overlap matrix elements  $T_{\mu\nu} = \langle \Phi_\mu | -\frac{1}{2}\nabla^2 | \Phi_\nu \rangle$ .
- The electron density  $\tilde{n}(\mathbf{r})$ .
- The compensation charge expansion functions  $\tilde{g}_L^a$ , which move rigidly with the atoms. Only those belonging to  $a$  change with  $\mathbf{R}^a$ .
- The zero potentials  $\bar{v}^a$  which also move rigidly with the atoms.
- The atomic density matrices  $D_{ij}^b$ .

The force is then

$$\mathbf{F}^a = -\frac{\partial E}{\partial \mathbf{R}^a}, \quad (7.4)$$

where<sup>1</sup>

$$\begin{aligned} \frac{\partial E}{\partial \mathbf{R}^a} = & \sum_{\mu\nu} \frac{\partial E}{\partial \rho_{\mu\nu}} \frac{\partial \rho_{\mu\nu}}{\partial \mathbf{R}^a} + \sum_{\mu\nu} \frac{\partial E}{\partial T_{\mu\nu}} \frac{\partial T_{\mu\nu}}{\partial \mathbf{R}^a} + \sum_L \int \frac{\delta E}{\delta \tilde{g}_L^a(\mathbf{r})} \frac{d\tilde{g}_L^a(\mathbf{r})}{d\mathbf{R}^a} d^3\mathbf{r} \\ & + \int \frac{\delta E}{\delta \tilde{n}(\mathbf{r})} \frac{\partial \tilde{n}(\mathbf{r})}{\partial \mathbf{R}^a} d^3\mathbf{r} + \int \frac{\delta E}{\delta \bar{v}^a(\mathbf{r})} \frac{d\bar{v}^a(\mathbf{r})}{d\mathbf{R}^a} d^3\mathbf{r} + \sum_{bij} \frac{\partial E}{\partial D_{ij}^b} \frac{\partial D_{ij}^b}{\partial \mathbf{R}^a}. \end{aligned} \quad (7.5)$$

Note that contrary to the grid-based case, the expression  $\frac{\partial D_{ij}^b}{\partial \mathbf{R}^a}$  which occurs in the last term may be nonzero even for  $a \neq b$ . This is because  $D_{ij}^b$  contains overlaps between projectors of atom  $b$  with basis functions on all other atoms, including  $a$ . In a related matter, many matrix element derivatives in other terms are in fact zero due to both or neither of the corresponding localized functions moving along with  $a$ , an issue which will be considered later. By not applying any assumptions about whether the basis functions move along with the atoms, we will obtain a universal result which is valid for any basis, atom-centered or not, which should reduce to the grid-based force expression under suitable simplifications.

<sup>1</sup>The use of hard  $d$  in the differential quotients involving radial functions such as  $\bar{v}^a$  expresses that the *functions* are taken to be functions of the atomic position (*only*).



## 7.2 Evaluation of force contributions

The force contributions from each of the partial derivatives in (7.5) will now be evaluated in turn.

### 7.2.1 State operator contribution

Our immediate problem is the derivatives of the coefficient matrices, which are unknown. Using the definition  $\frac{\partial E}{\partial \rho_{\mu\nu}} = H_{\nu\mu}$  and the generalized eigenvalue equation  $\mathbf{H}\mathbf{C} = \mathbf{S}\mathbf{C}\mathbf{\Lambda}$  and its adjoint (see Section 4.5, Equation (4.31)), we can rewrite:

$$\begin{aligned}
\sum_{\mu\nu} \frac{\partial E}{\partial \rho_{\mu\nu}} \frac{\partial \rho_{\mu\nu}}{\partial \mathbf{R}^a} &= \sum_{\mu\nu} H_{\nu\mu} \frac{\partial}{\partial \mathbf{R}^a} \sum_n c_{\mu n} f_n c_{\nu n}^* \\
&= \sum_{\mu\nu n} \left\{ \frac{\partial c_{\mu n}}{\partial \mathbf{R}^a} f_n c_{\nu n}^* H_{\nu\mu} + H_{\nu\mu} c_{\mu n} f_n \frac{\partial c_{\nu n}^*}{\partial \mathbf{R}^a} \right\} \\
&= \text{Tr} \left[ \frac{\partial \mathbf{C}}{\partial \mathbf{R}^a} \mathbf{F} \mathbf{C}^\dagger \mathbf{H} \right] + \text{Tr} \left[ \mathbf{H} \mathbf{C} \mathbf{F} \frac{\partial \mathbf{C}^\dagger}{\partial \mathbf{R}^a} \right] \\
&= \text{Tr} \left[ \frac{\partial \mathbf{C}}{\partial \mathbf{R}^a} \mathbf{F} \mathbf{\Lambda} \mathbf{C}^\dagger \mathbf{S} \right] + \text{Tr} \left[ \mathbf{S} \mathbf{C} \mathbf{\Lambda} \mathbf{F} \frac{\partial \mathbf{C}^\dagger}{\partial \mathbf{R}^a} \right] \\
&= \text{Tr} \left[ \mathbf{F} \mathbf{\Lambda} \left( \mathbf{C}^\dagger \mathbf{S} \frac{\partial \mathbf{C}}{\partial \mathbf{R}^a} + \frac{\partial \mathbf{C}^\dagger}{\partial \mathbf{R}^a} \mathbf{S} \mathbf{C} \right) \right]. \tag{7.6}
\end{aligned}$$

In the last step we have used that  $\mathbf{\Lambda}$  and  $\mathbf{F}$  are both diagonal matrices and therefore commute. Now consider the orthogonality condition (4.16), or  $\mathbf{C}^\dagger \mathbf{S} \mathbf{C} = \mathbf{I}$ . Its derivative with respect to  $\mathbf{R}^a$  must evidently be zero:

$$\frac{\partial \mathbf{C}^\dagger}{\partial \mathbf{R}^a} \mathbf{S} \mathbf{C} + \mathbf{C}^\dagger \frac{\partial \mathbf{S}}{\partial \mathbf{R}^a} \mathbf{C} + \mathbf{C}^\dagger \mathbf{S} \frac{\partial \mathbf{C}}{\partial \mathbf{R}^a} = \frac{\partial \mathbf{I}}{\partial \mathbf{R}^a} = \mathbf{0}. \tag{7.7}$$

This we can use to eliminate the dependence of (7.6) on coordinate matrix derivatives, obtaining

$$\sum_{\mu\nu} \frac{\partial E}{\partial \rho_{\mu\nu}} \frac{\partial \rho_{\mu\nu}}{\partial \mathbf{R}^a} = -\text{Tr} \left[ \mathbf{F} \mathbf{\Lambda} \mathbf{C}^\dagger \frac{\partial \mathbf{S}}{\partial \mathbf{R}^a} \mathbf{C} \right]. \tag{7.8}$$

Recall that the Lagrange multipliers after diagonalization of the Hamiltonian are Kohn-Sham energies,  $\lambda_{nn} = \epsilon_n$ , such that

$$\sum_{\mu\nu} \frac{\partial E}{\partial \rho_{\mu\nu}} \frac{\partial \rho_{\mu\nu}}{\partial \mathbf{R}^a} = -\sum_{n\mu\nu} \epsilon_n f_n c_{\mu n}^* \frac{\partial S_{\mu\nu}}{\partial \mathbf{R}^a} c_{\nu n}. \tag{7.9}$$

The derivative of the overlap matrix element  $S_{\mu\nu}$  is

$$\frac{\partial S_{\mu\nu}}{\partial \mathbf{R}^a} = \frac{\partial \Theta_{\mu\nu}}{\partial \mathbf{R}^a} + \sum_{bij} \Delta S_{ij}^b \left\{ \frac{\partial P_{i\mu}^{b*}}{\partial \mathbf{R}^a} P_{j\nu} + P_{i\mu}^{b*} \frac{\partial P_{j\nu}^b}{\partial \mathbf{R}^a} \right\}, \tag{7.10}$$

where  $\Theta_{\mu\nu} = \langle \Phi_\mu | \Phi_\nu \rangle$  and  $P_{i\mu}^b = \langle \tilde{p}_i^b | \Phi_\mu \rangle$ , and we have used that  $\Delta S_{ij}^b$  consists of internal atomic variables and thus is invariant to translation. By manipulating the summation indices the final result becomes

$$\begin{aligned} \sum_{\mu\nu} \frac{\partial E}{\partial \rho_{\mu\nu}} \frac{\partial \rho_{\mu\nu}}{\partial \mathbf{R}^a} &= - \sum_{n\mu\nu} c_{\nu n} \epsilon_n f_n c_{\mu n}^* \frac{\partial \Theta_{\mu\nu}}{\partial \mathbf{R}^a} \\ &\quad - 2\Re \sum_{n\mu\nu b i j} c_{\nu n} \epsilon_n f_n c_{\mu n}^* \frac{\partial P_{i\mu}^{b*}}{\partial \mathbf{R}^a} \Delta S_{ij}^b P_{j\nu}^b. \end{aligned} \quad (7.11)$$

### 7.2.2 Kinetic energy contribution

The kinetic energy contribution is simply

$$\sum_{\mu\nu} \frac{\partial E}{\partial T_{\mu\nu}} \frac{\partial T_{\mu\nu}}{\partial \mathbf{R}^a} = \sum_{\mu\nu} \rho_{\nu\mu} \frac{\partial T_{\mu\nu}}{\partial \mathbf{R}^a}. \quad (7.12)$$

### 7.2.3 Compensation charge contribution

The energy and the compensation charge basis functions can be related by using the chain rule. To this end, note first that the pseudo Hartree potential  $\tilde{v}_{\text{Ha}}$  is the derivative

$$\frac{\delta E}{\delta \tilde{\rho}(\mathbf{r})} = \tilde{v}_{\text{Ha}}(\mathbf{r}). \quad (7.13)$$

Second, choosing for the moment to perceive the charge as a functional of the pseudo density  $\tilde{n}$  along with all the compensation charges  $\tilde{Z}^b = \sum_{L'} Q_{L'}^b \tilde{g}_{L'}^b$ , we may write

$$\frac{\delta \tilde{\rho}[\tilde{n}, \{Q_{L'}^b, \tilde{g}_{L'}^b\}]}{\delta \tilde{g}_L^a} = \frac{\delta}{\delta \tilde{g}_L^a} \left[ \tilde{n} + \sum_{bL'} Q_{L'}^b \tilde{g}_{L'}^b \right] = Q_L^a. \quad (7.14)$$

Thereby

$$\sum_L \int \frac{\delta E}{\delta \tilde{g}_L^a(\mathbf{r})} \frac{d\tilde{g}_L^a(\mathbf{r})}{d\mathbf{R}^a} d^3\mathbf{r} = \sum_L \int \frac{\delta E}{\delta \tilde{\rho}(\mathbf{r})} \frac{\delta \tilde{\rho}(\mathbf{r})}{\delta \tilde{g}_L^a(\mathbf{r})} \frac{d\tilde{g}_L^a(\mathbf{r})}{d\mathbf{R}^a} d^3\mathbf{r} \quad (7.15)$$

$$= \int \tilde{v}_{\text{Ha}}(\mathbf{r}) \sum_L Q_L^a \frac{d\tilde{g}_L^a(\mathbf{r})}{d\mathbf{R}^a} d^3\mathbf{r}. \quad (7.16)$$

Notice that this result is essentially indifferent to the introduction of basis functions – the same formula applies when the wave functions are represented on a grid, the only difference being that the coefficients  $Q_L^a$  are ultimately evaluated differently.

### 7.2.4 Pseudo density contribution

The pseudo density is given by (4.21),

$$\tilde{n}(\mathbf{r}) = \sum_{\mu\nu} \rho_{\nu\mu} \Phi_\mu^*(\mathbf{r}) \Phi_\nu(\mathbf{r}) + \sum_b \tilde{n}_c^b(\mathbf{r}), \quad (7.17)$$

and we recall the definition  $\frac{\delta E}{\delta \tilde{n}(\mathbf{r})} = \tilde{v}_{\text{eff}}(\mathbf{r})$ . The pseudo core density  $\tilde{n}_c^b(\mathbf{r})$  is independent of  $\mathbf{R}^a$  except if  $a = b$ , so  $\tilde{n}_c^a(\mathbf{r})$  will be the only remaining core contribution. Thereby

$$\begin{aligned} \int \frac{\delta E}{\delta \tilde{n}(\mathbf{r})} \frac{\partial \tilde{n}(\mathbf{r})}{\partial \mathbf{R}^a} d^3\mathbf{r} &= \int \tilde{v}_{\text{eff}}(\mathbf{r}) \frac{d\tilde{n}_c^a(\mathbf{r})}{d\mathbf{R}^a} d^3\mathbf{r} \\ &+ \int \tilde{v}_{\text{eff}}(\mathbf{r}) \frac{\partial}{\partial \mathbf{R}^a} \sum_{\mu\nu} \rho_{\nu\mu} \Phi_\mu^*(\mathbf{r}) \Phi_\nu(\mathbf{r}) d^3\mathbf{r}, \end{aligned} \quad (7.18)$$

which can be rewritten to

$$\begin{aligned} \int \frac{\partial E}{\partial \tilde{n}(\mathbf{r})} \frac{\partial \tilde{n}(\mathbf{r})}{\partial \mathbf{R}^a} d^3\mathbf{r} &= \int \tilde{v}_{\text{eff}}(\mathbf{r}) \frac{d\tilde{n}_c^a(\mathbf{r})}{d\mathbf{R}^a} d^3\mathbf{r} \\ &+ 2\Re \sum_{\mu\nu} \rho_{\nu\mu} \int \frac{d\Phi_\mu^*(\mathbf{r})}{d\mathbf{R}^a} \tilde{v}_{\text{eff}}(\mathbf{r}) \Phi_\nu(\mathbf{r}) d^3\mathbf{r}. \end{aligned} \quad (7.19)$$

The former term is indifferent to the introduction of atomic basis functions (and therefore already handled in the grid code). The latter term is evaluated by integrating on the grid.

### 7.2.5 Zero potential contribution

The  $\bar{v}^a$  contribution is straightforwardly

$$\int \frac{\delta E}{\delta \bar{v}^a(\mathbf{r})} \frac{d\bar{v}^a(\mathbf{r})}{d\mathbf{R}^a} d^3\mathbf{r} = \int \tilde{n}(\mathbf{r}) \frac{d\bar{v}^a(\mathbf{r})}{d\mathbf{R}^a} d^3\mathbf{r}, \quad (7.20)$$

and is therefore not dependent on atomic basis set specifics.

### 7.2.6 Atomic density contribution

The *atomic hamiltonian* is defined to be the derivative

$$\Delta H_{ji}^a = \frac{\partial E}{\partial D_{ij}^a}, \quad (7.21)$$

and we know that the atomic density matrix (4.22) for some atom  $b$  is given by

$$D_{ij}^a = \sum_{\mu\nu} P_{i\mu}^b \rho_{\mu\nu} P_{j\nu}^{b*}. \quad (7.22)$$

Differentiating by  $\mathbf{R}^a$  for fixed  $\rho_{\mu\nu}$  yields

$$\frac{\partial D_{ij}^b}{\partial \mathbf{R}^a} = \sum_{\mu\nu} \rho_{\mu\nu} \left( \frac{\partial P_{i\mu}^b}{\partial \mathbf{R}^a} P_{j\nu}^{b*} + P_{i\mu}^b \frac{\partial P_{j\nu}^{b*}}{\partial \mathbf{R}^a} \right), \quad (7.23)$$

such that finally

$$\begin{aligned} \sum_{bij} \frac{\partial E}{\partial D_{ij}^b} \frac{\partial D_{ij}^b}{\partial \mathbf{R}^a} &= \sum_{bij\mu\nu} \Delta H_{ji}^b \rho_{\mu\nu} \left( \frac{\partial P_{i\mu}^b}{\partial \mathbf{R}^a} P_{j\nu}^{b*} + P_{i\mu}^b \frac{\partial P_{j\nu}^{b*}}{\partial \mathbf{R}^a} \right) \\ &= 2\Re \sum_{bij\mu\nu} \Delta H_{ji}^b \frac{\partial P_{i\mu}^b}{\partial \mathbf{R}^a} \rho_{\mu\nu} P_{j\nu}^{b*}, \end{aligned} \quad (7.24)$$

where the last expression can be obtained by either symmetry considerations or appropriate index shuffling.

### 7.3 General force expression

Combining all the equations (7.11), (7.12), (7.16), (7.19), (7.20) (7.24), we can behold the complete force expression

$$\begin{aligned}
\mathbf{F}^a = & -2\Re \sum_{b\mu\nu ij} \left\{ \Delta H_{ji}^b \rho_{\mu\nu} - \Delta S_{ji}^b \sum_n c_{\nu n} \epsilon_n f_n c_{\mu n}^* \right\} \frac{\partial P_{i\mu}^b}{\partial \mathbf{R}^a} P_{j\nu}^{b*} \\
& - \sum_{\mu\nu n} c_{\nu n} \epsilon_n f_n c_{\mu n}^* \frac{\partial \Theta_{\mu\nu}}{\partial \mathbf{R}^a} - \sum_{\mu\nu} \frac{\partial T_{\mu\nu}}{\partial \mathbf{R}^a} \rho_{\nu\mu} \\
& - 2\Re \sum_{\mu\nu} \rho_{\nu\mu} \int \frac{d\Phi_{\mu}^*(\mathbf{r})}{d\mathbf{R}^a} \tilde{v}_{\text{eff}}(\mathbf{r}) \Phi_{\nu}(\mathbf{r}) d^3\mathbf{r} - \int \tilde{v}_{\text{eff}}(\mathbf{r}) \frac{d\tilde{n}_c^a(\mathbf{r})}{d\mathbf{R}^a} d^3\mathbf{r} \\
& - \int \tilde{v}_{\text{Ha}}(\mathbf{r}) \sum_L Q_L^a \frac{d\tilde{g}_L^a(\mathbf{r})}{d\mathbf{R}^a} d^3\mathbf{r} - \int \tilde{n}(\mathbf{r}) \frac{d\tilde{v}^a(\mathbf{r})}{d\mathbf{R}^a(\mathbf{r})} d^3\mathbf{r}. \quad (7.25)
\end{aligned}$$

For mathematical clarity it may be worth noting that each of the terms involving an overlap derivative, even the first term for which this is not immediately obvious, can in fact be written as a matrix trace, which is useful when implementing the expression.

The overlap derivatives are written generically with respect to  $\mathbf{R}^a$  here. In this form, the force expression is true *in general*, i.e. for atomic orbital basis sets as well as, say, the real-space grid basis – the only difference being that the overlap derivatives are evaluated differently (most of them being zero for the grid basis, with the exception of the projector overlaps).

Accommodation of Bloch states is very straightforward. Since each type of overlap matrix is evaluated separately for each  $k$ -point, sums over  $k$ -points in the energy expressions (not included in this work; see the developer guide on the GPAW web page [24]) translate directly to sums over force contributions with  $k$ -point specific overlap matrices. Having multiple spins only affects the integration of the effective potential.

In adapting the force expression specifically to atom-centered basis functions, the overlap derivatives must be reexpressed in terms of interatomic separation vectors  $\mathbf{R}^b - \mathbf{R}^a$  rather than absolute positions, since the separation vectors are the natural variables of the two-center integral expressions (4.8). This will be done in the next section.

### 7.4 Derivatives of two-center integrals

To evaluate the overlap derivatives above, we must calculate the derivative of the two-center integral expansions (4.8). It proves convenient to transfer a factor of  $R^l$  from the radial part to the formerly angular part, wherefore we define

$$\bar{\Theta}_{lm}(R) = \frac{\Theta_{lm}(R)}{R^l}, \quad (7.26)$$

$$\bar{Y}_{lm}(\mathbf{R}) = R^l Y_{lm}(\hat{\mathbf{R}}). \quad (7.27)$$

The functions  $\bar{Y}_{lm}(\mathbf{R})$  are called the *real solid spherical harmonics*, and the advantage is that these are just polynomials in the cartesian coordinates. Then

the overlap integral takes the form

$$\Theta(\mathbf{R}) = \sum_L \Theta_L(R) Y_L(\hat{\mathbf{R}}) = \sum_L \bar{\Theta}_L(R) \bar{Y}_L(\mathbf{R}). \quad (7.28)$$

Differentiation with respect to  $\mathbf{R}$  yields

$$\begin{aligned} \frac{d\Theta(\mathbf{R})}{d\mathbf{R}} &= \sum_L \left\{ \frac{d\bar{\Theta}_L(R)}{d\mathbf{R}} \bar{Y}_L(\mathbf{R}) + \bar{\Theta}_L(R) \frac{d\bar{Y}_L(\mathbf{R})}{d\mathbf{R}} \right\} \\ &= \sum_L \left\{ \frac{d\bar{\Theta}_L(R)}{dR} \bar{Y}_L(\mathbf{R}) \hat{\mathbf{R}} + \bar{\Theta}_L(R) \frac{d\bar{Y}_L(\mathbf{R})}{d\mathbf{R}} \right\}, \end{aligned} \quad (7.29)$$

where we have used that if  $r^2 = x^2 + y^2 + z^2$ , then  $\frac{dr}{dx} = \frac{x}{r}$  and so on. In this form all variables are trivially evaluated – the radial splines, being piecewise polynomials, have piecewise polynomial derivatives as well.

Differentiation of an overlap with respect to a particular nuclear coordinate  $\mathbf{R}^a$  works out somewhat differently depending on matters of localized function ownership: if e.g. both or none of the localized functions reside on the atom in question, the overlap is translation invariant. We can write down the following four cases, letting  $\mathbf{R}^\mu$  designate the location of whichever atom the  $\mu$ 'th function belongs to:

$$\frac{\partial \Theta_{\mu\nu}(\mathbf{R}^\nu - \mathbf{R}^\mu)}{\partial \mathbf{R}^a} = \begin{cases} \mathbf{0} & \mu \in a, \nu \in a \\ -\frac{d\Theta_{\mu\nu}}{d\mathbf{R}^{\mu\nu}} & \mu \in a, \nu \notin a \\ \frac{d\Theta_{\mu\nu}}{d\mathbf{R}^{\mu\nu}} & \mu \notin a, \nu \in a \\ \mathbf{0} & \mu \notin a, \nu \notin a \end{cases} \quad (7.30)$$

where set inclusion denotes atomic ownership. We can then rewrite each of the overlap derivative expressions in (7.25):

$$\sum_{\mu\nu} \frac{\partial \Theta_{\mu\nu}}{\partial \mathbf{R}^a} \rho_{\nu\mu} = \sum_{\substack{\mu \in a \\ \nu \notin a}} \frac{\partial \Theta_{\mu\nu}}{\partial \mathbf{R}^a} \rho_{\nu\mu} + \sum_{\substack{\mu \notin a \\ \nu \in a}} \frac{\partial \Theta_{\mu\nu}}{\partial \mathbf{R}^a} \rho_{\nu\mu} \quad (7.31)$$

$$= - \sum_{\substack{\mu \in a \\ \nu \notin a}} \frac{d\Theta_{\mu\nu}}{d\mathbf{R}^{\mu\nu}} \rho_{\nu\mu} + \sum_{\substack{\mu \notin a \\ \nu \in a}} \frac{d\Theta_{\mu\nu}}{d\mathbf{R}^{\mu\nu}} \rho_{\nu\mu}. \quad (7.32)$$

The former term can be rewritten by interchanging symbols, then reversing the atomic separation vector:

$$- \sum_{\substack{\mu \in a \\ \nu \notin a}} \frac{\partial \Theta_{\mu\nu}}{\partial \mathbf{R}^{\mu\nu}} \rho_{\nu\mu} = - \sum_{\substack{\mu \notin a \\ \nu \in a}} \frac{\partial \Theta_{\nu\mu}}{\partial \mathbf{R}^{\nu\mu}} \rho_{\mu\nu} = \sum_{\substack{\mu \notin a \\ \nu \in a}} \frac{\partial \Theta_{\mu\nu}^*}{\partial \mathbf{R}^{\mu\nu}} \rho_{\nu\mu}^*, \quad (7.33)$$

which yields the final expression

$$\sum_{\mu\nu} \frac{\partial \Theta_{\mu\nu}}{\partial \mathbf{R}^a} \rho_{\nu\mu} = 2\Re \sum_{\substack{\mu \notin a \\ \nu \in a}} \frac{d\Theta_{\mu\nu}}{d\mathbf{R}^{\mu\nu}} \rho_{\nu\mu}. \quad (7.34)$$

Using this, the summation sets for the overlaps appearing in (7.25) can be reduced significantly. On a technical note, we have not yet implemented this

final expression for the overlaps, but instead use the general force expression (7.25) with the modification that a “mask” is applied to each overlap matrix, multiplying the elements by 0, 1 or -1 according to (7.30). While this is obviously not efficient, it can be useful because it allows direct finite-difference checks of all overlap matrices.

## 7.5 Force test calculations

Having implemented Equation (7.25), this section aims to document that the force is, in fact, calculated correctly. For this reason we run two tests. First a simple check demonstrating that the calculated forces are reproduced by finite-difference calculations in the general case of multiple  $k$ -points, and periodic boundary conditions, then and a more comprehensive but gamma-point only *egg-box* force test, which will be explained later.

Before we start, a useful initial test is to check that the calculated forces have the correct symmetries and that they obey Newton’s 3rd law, i.e. that the sum of all forces on all atoms must be zero for each direction. Interestingly, it turns out that:

- Each of the force contributions involving derivatives with respect to the state operator, kinetic energy and atomic density matrices *separately* sums up to zero with very high precision.
- The sum of all the remaining force terms, i.e. those involving the effective potential and all terms that relate to compensation charges and zero potential, must then also be zero in order for the result to obey Newton’s 3rd law. This is also the case, although each of these terms separately does *not* add up to zero. Furthermore the agreement is not as accurate as for the above terms. The small deviation from Newton’s 3rd law during any force calculation is caused largely by these terms.

### 7.5.1 Finite-difference checks

The easy way of testing calculated forces is by finite-difference. We use the symmetric finite-difference approximation

$$F_x^a \approx -\frac{E(x + \Delta x) - E(x - \Delta x)}{2\Delta x} \quad (7.35)$$

and compare this to the calculated forces. Table 7.1 shows forces calculated using Equation (7.25) as well as finite-difference. The system under consideration is the diamond structure accessible in `gpaw.utilities.bulk`, except the first atom at (0,0,0) is shifted by -0.1 Angstroms along all three axes, such that the forces are non-zero. The non-trivial parameters are listed in Table 7.2. With four atoms, three cartesian directions and two energy evaluations per atomic force component, the total number of energy evaluations for a finite-difference calculation is 24. Each calculation uses a new calculator object rather than reusing the previous density, which takes more time but guarantees that there is no systematical bias. Evidently the numbers agree very well, thus demonstrating that the implementation very probably works.

Calculated forces [eV/Å]						
Localized basis sets				Grid-based wave functions		
Atom	$F_x$	$F_y$	$F_z$	$F_x$	$F_y$	$F_z$
1	5.29607	2.73416	4.95862	5.11187	2.65237	4.72001
2	-1.36114	-1.57156	-1.35054	-1.30671	-1.46240	-1.35617
3	-1.35456	-0.10720	-0.03019	-1.35063	-0.10693	-0.02625
4	-2.58200	-1.05918	-3.58148	-2.45308	-1.08390	-3.33826

Finite-difference forces [eV/Å]						
Localized basis sets				Grid-based wave functions		
Atom	$F_x$	$F_y$	$F_z$	$F_x$	$F_y$	$F_z$
1	5.29391	2.73727	4.95631	5.13250	2.65212	4.72042
2	-1.36292	-1.57049	-1.35015	-1.30683	-1.46227	-1.35642
3	-1.35217	-0.10762	-0.02952	-1.37083	-0.10678	-0.02636
4	-2.58162	-1.06121	-3.57841	-2.45353	-1.08377	-3.31776

Calculated forces minus finite-difference forces [eV/Å]						
Localized basis sets				Grid-based wave functions		
Atom	$F_x$	$F_y$	$F_z$	$F_x$	$F_y$	$F_z$
1	0.00216	-0.00311	0.00231	-0.02063	0.00025	-0.00041
2	0.00178	-0.00107	-0.00039	0.00012	-0.00013	0.00025
3	-0.00239	0.00042	-0.00067	0.02020	-0.00015	0.00011
4	-0.00038	0.00203	-0.00307	0.00045	-0.00013	-0.02050

**Table 7.1:** Forces calculated by differentiation compared to finite-difference results calculated using LCAO as well as real-space grid basis. The system is a perturbed diamond crystal with four atoms per cell.

Parameter	Value
Cell [Å]	(3.57, 2.52, 2.52)
Periodic	yes
Grid spacing	0.15 Å
$k$ -points	(2, 4, 4)
Basis	DZP
FD step $\Delta x$	0.001 Å

**Table 7.2:** Parameters in finite-difference force test. Any parameters not mentioned here are default values.

### 7.5.2 Egg-box forces

In order to remove any remaining doubt about whether this works or not, we perform a somewhat more comprehensive test, namely checking that the calculated forces reproduce the slope of the energy curve resulting from the *egg-box effect*, which we shall now explain briefly.

Suppose we have a system consisting of any constellation of atoms inside a periodic cell. Physically, the energy of this system is of course translation invariant. However, due to the finite grid resolution, translation is not a true symmetry operation, except when translating by an integer times the grid spacing. Thus the energy will in general, as the system is gradually translated, oscillate with a spatial frequency corresponding to the grid resolution. This is called the *egg-box effect*, owing to the energy curve oscillating like the lid of an egg box.

Consider a single atom in a periodic cell, using some grid spacing  $h$ . Then select a set of dislocations  $x_i$ , where  $0 \leq x_i \leq h/2$ , and calculate the energy  $E(x_i)$  and the force component  $F_x(x_i)$  of the system translated by each of those amounts. At each point the linearization

$$E(x + dx) - E(x) = -F(x) dx \quad (7.36)$$

must apply, i.e. the line segments through each point  $(x_i, E(x_i))$  with slope  $F_x(x_i)$  must connect neighbouring points such as  $(x_{i+1}, E(x_{i+1}))$ .

Figure 7.1 shows an egg-box force test on a hydrogen atom. The test uses the default DZP basis.<sup>2</sup> The line segments join the calculated energy points quite well in most locations. Curiously, the first couple of points tend to vary discontinuously. This is probably because the energies are calculated “left to right” on the graph, using the same calculator object. The translated density of the previous calculation is then used as an initial guess for the next calculation: after the first calculation it may not have converged as well as in the succeeding ones, which becomes more important when considering very small energy differences as is the case here. This is might be more important for the LCAO-based calculations, which use a somewhat more lax stop criterion by default.<sup>3</sup> For some reason the central part of the middle ( $h = 0.1750$ ) plot appears slightly off in both the grid and LCAO cases, which *might* also be helped by improving the convergence criteria, though we cannot really explain this; at the very least it is not specific to the use of atomic basis functions.

This test has been run on a number of different atoms, Al, C, Cl, F, H, Li, N, O, S and Si, obtaining similar results.

## 7.6 Summary

We have by now derived a formula for the total force on an atom which is in principle valid for any basis set. With atom-centered basis sets, this involves

<sup>2</sup>The test can be performed by executing `dimer.py --lcao=dzp H`, where the test programme resides in `gpaw.testing`, if an appropriate DZP basis set is available.

<sup>3</sup>For LCAO calculations, the change in density per Kohn-Sham iteration is used as stop criterion, whereas in the grid-based case, changes in density as *well as wave functions* are considered, since the wave functions too are subject to iteration here and thus have to converge as well.



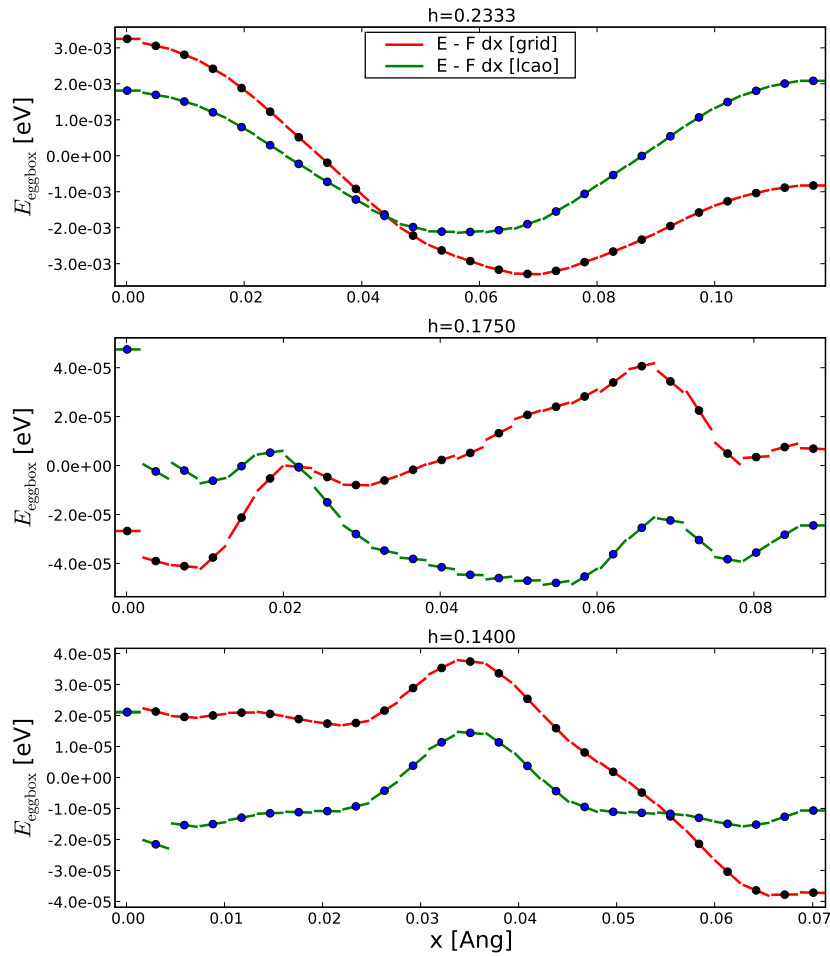


**Figure 7.1:** *Egg-box* force test for hydrogen with different grid spacings  $h$ . The dots are calculated energies as a function of the sub-resolution displacement  $x$ . The line segments are given by  $E(x) - F(x) dx$  extrapolated around each point. The red/black curves represent grid-based calculations while the blue/green ones use localized basis functions. The energy zero is arbitrary.

derivatives of localized function overlaps, which are calculated from the two-center integral expansions.

The formula has been implemented in GPAW and subsequently tested by comparing calculated forces with finite-difference approximations. This was done with periodic boundary conditions with multiple  $k$ -points. We have further shown that the forces correctly account for the very small egg-box effect, meaning that the calculated forces are highly accurate.

## Chapter 8

# Conclusion

We have derived a variational problem and corresponding Kohn-Sham equations valid in the projector augmented wave method when using localized basis sets. This has been implemented in the real-space grid-based GPAW code. In using localized functions, grid-based integrations are replaced by two-center integrals which can be expressed as radial splines times spherical harmonics.

A basis set generator has been implemented which is capable of generating multiple-zeta basis sets plus polarization functions. Basis sets consist of one pseudoatomic orbital for each valence state, which is generated by solving the Kohn-Sham equations for an isolated atom. Smooth shape is achieved by applying the reversed PAW transformation on the all-electron Kohn-Sham solutions.

Multiple-zeta basis sets can be generated by the split-valence-like method employed in SIESTA, or by means of an energy derivative of the pseudoatomic functions. So far we have found the former method to produce better results. Angular flexibility is improved by adding polarization functions. We have implemented a method to generate polarization functions by interpolating the polarized character of the wave function for a given reference system. Observing that the generated functions share a certain universal shape, it turns out that they can generally be represented by a single Gaussian-like function.

Calculations on simple molecules show that double-zeta polarized basis sets are required and in many cases sufficient to obtain reasonably converged atomization energies. We find calculations of adsorption energies to deviate quite considerably from grid results, which is likely due to the basis set superposition error. This can probably be improved in the near future by the implementation of “ghost orbitals”, which prevent the basis set superposition error by ensuring that different calculations are done in the same Hilbert space.

Finally, we have derived an expression for the force acting on an atom, which will enable geometry relaxations and molecular dynamics simulations. The calculated forces reproduce finite-difference results and the egg-box effect very accurately.



# Bibliography

- [1] P. Hohenberg, W. Kohn. *Inhomogeneous Electron Gas*. Phys. rev. **136**, B864, 1964.
- [2] W. Kohn. Nobel lecture: *Electronic structure of matter—wave functions and density functionals*. Reviews of Modern Physics, Vol. **71**, No. 5. 1999.
- [3] W. Kohn and L. J. Sham. *Self-consistent equations including exchange and correlation effects*. Phys. Rev. **140**, B1133, 1965.
- [4] J.P. Perdew, K. Burke, M. Ernzerhof. *Generalized gradient approximation made simple*. Phys. Rev. Lett., Vol. **77**, 3865. 1996.
- [5] D. Vanderbilt. *Soft self-consistent pseudopotentials in a generalized eigenvalue formalism*. Phys. Rev. B **41**, 7892 (1990)
- [6] L. Kleinman, D.M. Bylander. *Efficacious form for model pseudopotentials*. Phys. Rev. Lett. **48**, 1425. 1982.
- [7] G. Kresse, D. Joubert. *From ultrasoft pseudopotentials to the projector augmented-wave method*, Phys. Rev. B **59**, 1758, (1999).
- [8] Peter E. Blöchl. *Projector augmented-wave method*. Phys. Rev. B **50** 17953
- [9] Peter E. Blöchl, Clemens J Först, Johannes Schimpl. *Projector augmented wave method: ab initio molecular dynamics with full wave functions*, Bull. Mater. Sci., Vol. **26**, No. 1, Jan. 2003, pp. 33–41.
- [10] J. J. Mortensen, L. B. Hansen, K. W. Jacobsen. *Real-space grid implementation of the projector augmented wave method*, Phys. Rev. B **71**, 035109 (2005).
- [11] J.M. Soler, E. Artacho, J.D. Gale, A. García, J. Junquera, P. Ordejón, D. Sánchez-Portal. *The SIESTA method for ab initio order- $N$  materials simulation*. J. Phys.: Condens. Matter **14** (2008) 2745-2779.
- [12] E. Artacho, D. Sánchez-Portal, P. Ordejón, A. García, J. M. Soler. *Linear-Scaling ab-initio Calculations for Large and Complex Systems*. phys. stat. sol. (b) **215**, 809 (1999)
- [13] J. Junquera, O. Paz, D. Sánchez-Portal, E. Artacho. *Numerical atomic orbitals for linear-scaling calculations*. Phys. Rev. B **64** 235111.

- [14] Michele Gusso. *Study on the maximum accuracy of the pseudopotential density functional method with localized atomic orbitals versus plane-wave basis sets*, J. Chem. Phys. **128**, 044102 (2008).
- [15] E. Artacho, E. Anglada, O. Diéguez, J.D. Gale, A. García, J. Junquera, R.M. Martin, P. Ordejón, J.M. Pruneda, D. Sánchez-Portal, J.M. Soler. *The SIESTA method; developments and applicability*. J. Phys.: Condens. Matter **20** (2008) 064208
- [16] S. Kurth, J. P. Perdew and P. Blaha: *Molecular and Solid State Tests of Density Functional Approximations: LSD, GGAs, and Meta-GGAs*. Int. J. Quant. Chem. 75, 889-898. 1999.
- [17] Marco Vanin: *Projector Augmented Wave Calculations with Localized Atomic Orbitals*. Master thesis, written at CAMD, 2008.
- [18] W.H. Press, B.P. Flannery, S.A. Teukolsky, W.T.Vetterling. *Numerical Recipes in C: The Art of Scientific Computing*, Cambridge University Press. 1988.
- [19] Richard M. Martin. *Electronic Structure: Basic Theory and Practical Methods*. Cambridge University Press, 2004.
- [20] Leslie E. Ballentine. *Quantum mechanics*. World scientific publishing, 1998.
- [21] B. H. Bransden, C. J. Joachain. *Quantum mechanics*, 2nd Edition.
- [22] S. R. Elliot. *The Physics and Chemistry of Solids*. John Wiley & Sons.
- [23] Nakhle Asmar. *Partial Differential Equations and Boundary Value Problems*, 4th Edition.
- [24] GPAW website  
<https://wiki.fysik.dtu.dk/gpaw/>
- [25] Dacapo website  
<https://wiki.fysik.dtu.dk/dacapo/>
- [26] CAMPOS website  
<https://wiki.fysik.dtu.dk/>
- [27] SIESTA website  
<http://www.uam.es/departamentos/ciencias/fismateriac/siesta/>
- [28] GAUSSIAN website  
<http://gaussian.com/>